

AD-753 844

MEASUREMENT OF ELASTIC MODULI OF
MATERIALS AT ELEVATED TEMPERATURE

E. P. Papadakis, et al

Panametrics, Incorporated.

Prepared for:

Office of Naval Research

14 November 1972

DISTRIBUTED BY:

NTIS

National Technical Information Service
U. S. DEPARTMENT OF COMMERCE
5285 Port Royal Road, Springfield Va. 22151



PANAMETRICS

221 Crescent Street • Waltham, Massachusetts 02154 • (617) 899-2719

Measurement of Elastic Moduli of Materials at Elevated Temperature

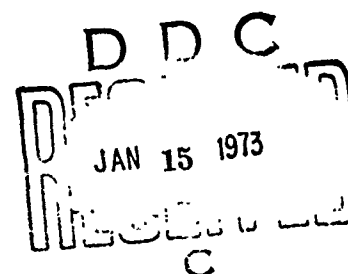
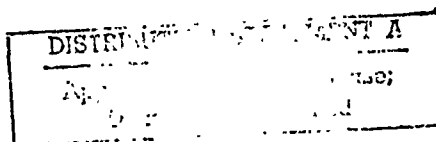
Progress Report for the 1st Quarterly
Period Ending November 14, 1972

Performed for
Office of Naval Research
under
Contract N00014-73-C-0023
I. D. No. NR 384-320/04-27-72/468

Prepared by
E. P. Papadakis
K. A. Fowler
L. C. Lynnworth
E. H. Carnevale
J. Chen

Reproduced by
NATIONAL TECHNICAL
INFORMATION SERVICE
U S Department of Commerce
Springfield VA 22151

Reproduction in whole or in part is permitted for any purpose of the
United States Government.



65

AD753844

I. BACKGROUND

This work was supported by the Office of Naval Research under Contract N00014-73-C-0023, ONR Contract Authority Identification Number NR 384-320/04-27-72/468.

II. DISCUSSION

The work reported here is a continuation of the research conducted under our former Contract N00014-71-C-0050. Both theoretical and experimental work has been undertaken. Progress in several areas is summarized below.

A. Attenuation Compensation for Measuring Ultrasonic Velocity at High Temperatures in One or More Segments of Wire

Since attenuation increases with temperature, particularly above half the melting point (absolute scale), it is necessary to compensate for attenuation to assure echoes of large enough amplitude to measure when working with wires immersed in a hot environment. A method is outlined to calculate the echo amplitudes desirable at room temperature in order to fabricate a wire-sonic transmission line for operation at high temperatures for velocity measurements. Applications to ultrasonic thermometry are mentioned.

B. Versatile Ultrasonic Facility for Operation to 1000°C

To facilitate measurements on wires and thin rods from room temperature to 1000°C, a simple and versatile vacuum furnace and heat controller have been built. An ultrasonic port allows the entrance of several wire transmission lines and a thermocouple. Ultrasonic measurements of modulus and attenuation can be made.

C. Measurements on Remendur to 1000°C

In the vacuum furnace mentioned above, measurements of Young's modulus and the attenuation of extensional ultrasonic waves have been made to 1000°C in Remendur, a magnetostrictive iron/cobalt alloy. It was desired to study magnetostrictive metals up to and beyond the Curie temperature. Further measurements are planned.

D. Statistical Errors in Attenuation and Reflection Coefficient

Statistical methods have been used to determine the errors to be expected in measuring the attenuation α in a specimen of length L and the reflection coefficient R at a buffer/specimen interface (or lead-in-wire/wire-specimen joint) with traveling wave methods. Formulas are derived for the maximum (3σ) errors in R and $2\alpha L$.

E. Momentary Contact Experiments for Moduli and Attenuation at Elevated Temperatures

We are preparing to experiment further with superalloys at elevated temperatures. The next alloy to be tested will be Waspalloy, a structural metal used at high temperatures.

F. Polymerization of Plastics

Our work on testing the curing of epoxy resins has been written up for technical publication; the text appears as Appendix A. The paper has application to various plastics and coatings, and possibly to solids during melting and freezing.

G. Nomogram for Attenuation and Reflection Coefficient

To familiarize the scientific and engineering community with the utility of making ultrasonic attenuation measurements by ultrasonic traveling wave methods using buffer rods or lead-in wires, a letter has been prepared for publication showing a nomogram for obtaining the attenuation and the reflection coefficient from the amplitudes of three echoes. This letter is given in Appendix B.

H. Ultrasonic Velocity in Sheet Material

Ultrasonic velocity in sheet material can be used to measure or monitor the moduli of the material. Various production variables might be brought under closer control if the moduli of sheets could be monitored. A set of experiments was performed on various types of paper to investigate wave propagation in a material both high in attenuation and highly anisotropic. A paper was written summarizing these measurements and reviewing some foreign and domestic work. This paper appears as Appendix C. It is felt that other types of sheet material could be monitored at high temperatures by ultrasonics.

III. DETAILS OF WORK

A. Attenuation Compensation for Measuring Ultrasonic Velocity at High Temperatures in One or More Segments of Wire

In certain experiments, one may be interested in measuring the ultrasonic propagation constants along one or more segments of a wire waveguide. For example, one may wish to compare the response of two or more different materials, e. g., pure Re, pure Mo, and Re/Mo alloys, in a given thermal and/or nuclear environment. Alternatively, one may wish to use a given material, e. g., Re, to sense the variation or profile of an environmental parameter such as temperature or neutron fluence.

At temperature below about half the absolute melting temperature, $T < 0.5 T_M$, the attenuation coefficient α at frequencies well below 1 MHz is usually small enough so that detectable echoes can be obtained¹ even when the sound pressure reflection coefficient R is much less than unity; e. g., $R \approx 0.1$. In this case at least 10 and possibly 20 segments can be monitored by a single transducer.

On the other hand, at temperature above $\sim 0.5 T_M$, α may increase by more than 1 order of magnitude. To provide sufficiently strong echoes, one may have to divide the available ultrasonic energy among a smaller number of segments, e. g., 5 or less. Correspondingly, the R 's at segment interfaces need to be increased.

The problem, then, is to optimize the choices of R_i , for a given set of αL_i 's, where the L_i 's are the lengths of the segments.

Let us define "optimum" to be that set of R_i and L_i which yields essentially equal magnitude echoes at the expected conditions of maximum attenuation, and minimum or tolerable interference echoes at temperatures well below $0.5 T_M$. To illustrate one approach to this optimization procedure, let us analyze the case where temperature is uniform over the segments, and high enough above $0.5 T_M$ so that very small, identical R 's such as $R = 0.1$ will not suffice. Further, since moderately large R 's will be large enough to yield interfering reverberations, the lengths of adjacent segments need to be unequal.^{2,3}

The temperature dependence of α in Re is shown in Fig. 1. It is seen that α increases sharply above about 1600°C from 0.005 Np/cm (4.34 dB/m) to 0.03 Np/cm (26 dB/m) at 2000°C . An α of 0.015 Np/cm (10 dB/m) occurs near 1650°C . On a normalized (homologous) temperature scale, 1650°C translates to $\approx 0.56 T_M$.

In Fig. 2 we plot lines of positive slope, for several α 's. Let us use this graph to determine R_i . For simplicity, suppose we are to operate at a maximum temperature of 1650°C , i. e., $\alpha = 10 \text{ dB/cm}$. Further, suppose we are to utilize a waveguide containing four segments of alternating lengths $L_i = 30, 20, 30, 20 \text{ cm}$, as shown in Fig. 3. If the echoes A, B, C, D, E are to be equal at 1650°C , their relative amplitudes at room temperature may be obtained from Fig. 2, remembering that each segment attenuates the signal by $e^{-2\alpha L_i}$: 0.199, 0.316, 0.631, and 1.000 V.

Starting with echo E at the free end, we may proceed to compute R_i and then compute corresponding diameter ratios.

Results are tabulated in Table I. A comparison with cases where α is negligibly small, as well as where α is substantially larger than 10 dB/m , is given in Table II.

In principle, a rod containing diameter steps as required by Table I could be fabricated by centerless "plunge" grinding; by welding together segments of the required diameters; by electric discharge machining; by drawing; or by other means. Figure 4 is included to illustrate that stepped-diameter wires can in fact be built, and when heated, provide a detectable echo pattern. However, once we have calculated the R_i 's, we may produce the reflections by means other than stepping the diameters of each complete segment. For example, circumferential grooves or added masses such as weld-upset bumps may be used (Fig. 5).¹ In some materials, another alternative is drilling axial holes of appropriate diameters and depths.

Details on the calculation of R_i and diameter ratios are given next, using the notation of Fig. 3.

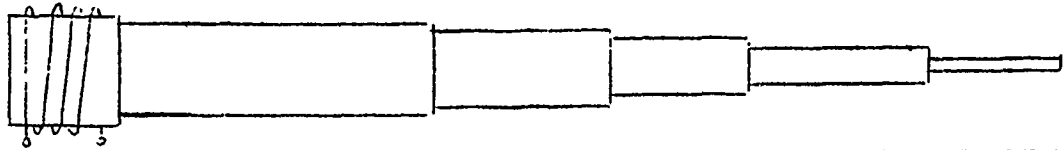
For the end segment,

$$\frac{D}{E} = \frac{R_D}{R_E} \frac{1}{T_{34} T_{43}} = \frac{-R_D}{T_{34} T_{43}} \equiv \frac{0.631}{1.0} \quad (1)$$

since $R_E = -1$ at the free end.

$$\text{But} \quad R_D = \frac{r_{34} - 1}{r_{34} + 1} \quad (2)$$

Table I

Parameters calculated for segmented line of one material					
					
Segment	-	1	2	3	4
Diameter					
Notation	D_0	D_1	D_2	D_3	D_4
Relative (mm)	2.36	2.30	2.05	1.69	1.00
Diameter (in.)	0.0943	0.0918	0.0818	0.0675	0.040
Length L_i (cm)	-	30	20	30	20
Round-Trip Attenuation (dB) - if $\alpha = 10$ dB/m		6	4	6	4
Required Relative Echo Amplitude at Room Temp, V	0.100	0.199	0.316	0.631	1.000
Sound Pressure Refl. Coef. R	-0.0262	-0.1175	-0.19	-0.483	-1.000
Transmission*					
Coef. \overrightarrow{T}	0.973	0.883	0.81	0.517	0
Transmission Coef. \overleftarrow{T}	1.02	1.115	1.19	1.49	0

*Arrows over T signify direction of propagation.

Table II

Comparison of segmented lines having relatively low, medium and high attenuation			
Attenuation	Low	Medium	High
Typical $ R $	< 0.1	~ 0.1 to 0.5	≥ 0.5
No. of segments	≥ 10	≤ 5	2
Relative lengths	Equal	Adjacent segments unequal, but alternate segments may be equal	Unequal
Mode	Extensional or torsional	Extensional or torsional	Extensional and/or torsional

where $r_{24} = Z_4/Z_3 = (D_4/D_3)^2 = \frac{1+R}{1-R}$ (3)

and $T_{34} = \frac{2r_{34}}{r_{34}+1}$, $T_{43} = \frac{2/r_{34}}{1/r_{34}+1} = \frac{2}{1+r_{34}}$ (4)

and so $T_{34} T_{43} = \frac{4r_{34}}{(r_{34}+1)^2}$ (5)

Therefore $R_D = \frac{r_{34}-1}{r_{34}+1} = \frac{(-0.631)(4r_{34})}{(r_{34}+1)^2}$ (6)

from which $r_{34} = 0.35 \equiv (D_4/D_3)^2$ (7)

or $D_4/D_3 = 0.592$; $D_3/D_4 = 1.69$ (8)

and $R_D = -0.483$ (9)

Proceeding towards the transducer, we write

$$\frac{C}{D} = \frac{R_C}{R_D} \frac{1}{T_{23} T_{32}} \equiv \frac{0.316}{0.631} = 0.502 \quad (10)$$

This leads to an equation of the form

$$\frac{r_{23}-1}{r_{23}+1} = \frac{(0.502)(-0.483)(4r_{23})}{(r_{23}+1)^2} \quad (11)$$

having a solution $r = 0.68$ from which

$$D_3/D_2 = 0.826 \quad (12)$$

and $R_C = -0.19$, $T_{23} = 0.81$, $T_{32} = 1.19$ (13)

For the next segment we similarly write

$$\frac{B}{C} = \frac{R_B}{R_C} \frac{1}{T_{12} T_{21}} = \frac{0.199}{0.316} = 0.63 \quad (14)$$

which leads to $D_2/D_1 = 0.891$, $R_B = -0.1175$, $T_{12} = 0.883$, $T_{21} = 1.115$.

For the fourth segment,

$$\frac{A}{B} = \frac{R_A}{R_B} \frac{1}{T_{01} T_{10}} = \frac{0.100}{0.199} = 0.5 \quad (15)$$

from which there results

$$D_1/D_0 = 0.975 \quad (16)$$

The Remendur transducer diameter may be made large enough to impedance match to the Re diameter D_0 , or, alternatively, the Re may be tapered down to match a given Remendur diameter.

Details on transducer construction,⁵ self-heating of Re to T_M ,⁶ and scanning segmented lines to measure selected echo pairs⁷ have been described elsewhere, and so are not repeated here.

From Fig. 3 and Table I it is seen that the magnitude of the R_i 's increases monotonically from 0 at the transducer/lead-in joint to unity at the free end. From the tabulated transmission and reflection coefficients, and assuming $\alpha = 0$ and then $\alpha = 10$ dB/m, we can calculate the amplitudes of the interfering reverberations such as B' , C' , B'' , C'' . The formulas are of the form $B' = -BR_A R_B e^{-2\alpha L_1}$ and $C' = CR_B R_C e^{-2\alpha L_2}$.

B' and C' are inverted, and are straddled by C and D . B'' and C'' are not inverted, and under isothermal conditions, coincide and therefore add, midway between D and E . Their values relative to $E \equiv +1$ V are given in Table III. It is seen that these reverberations are smaller than the next desired echoes by about 2 or more orders of magnitude. Therefore the diameter ratios calculated above satisfy the given optimization criterion.

Table III

Amplitudes of interfering echoes relative to $E = +1$ Volt		
Interfering Echo	Amplitude, millivolts	
	$\alpha = 0$ dB/m	$\alpha = 10$ dB/m
B'	-0.613	-0.306
B''	+0.002	+0.001
C'	-7.05	-4.34
C''	+0.157	+0.099

Regarding Fig. 5, we note that when the coil (transducer) is near the center of the line containing circumferential "bumps" and "grooves," (see bottom oscillogram) the echoes show corresponding polarities from both sets of discontinuities. However, when the coil is moved to either end,⁵ the echoes from the closer set may be lost in the recovery transient, and so, after recovery, one observes a set of like echoes from the remote segments. Again, these echoes are due to $|R_i|$'s small enough so reverberations in the segments are small enough not to interfere. While the oscillogram traces in Fig. 5 were generated using a Remendur demonstration line of length less than 1 m, one could construct a much longer line, ~ 10 to 100 m, if clearer separation of bipolar echoes, detected with a near-center transducer, were desired.

We may further note in Fig. 5 an "apparent" polarity reversal for bumpy or groovy echoes, when the coil is moved from either end to the center. This illusion is due to what appears as a phase-reversing effect of the reinforcing end echo, when the coil is at the end.⁵ Careful examination of the slope of the leading edge of the echoes will show, however, that the leading edge retains its polarity, when the coil is moved from the center to the end of the line.

B. Versatile Ultrasonic Facility for Operation to 1000°C

The system for operating to 1000°C consists of an evacuated quartz glass tube heated at its central portion by a clamshell furnace. The furnace (Hevi Duty Electric Company Type M-2012) is controlled manually with 20 Amp Variac connected as shown in Fig. 6. The power source was mounted in a portable console for safety and convenience. Temperature is monitored with a chromel alumel thermocouple connected to a Leeds & Northrup potentiometer. Inside the furnace, a steel cell is built to keep even temperature over the entire volume.

The quartz glass tube shown in Fig. 7 is evacuated by a roughing pump. Baffles are put on both ends of the tube to keep the radiant energy from damaging the vacuum seals at the ends of the tube.

Tungsten wires are used as lead-in which go through a Conax vacuum seal into the cell as described in Fig. 7. Inside the cell a steel rack is used to support the samples. Very thin steel wire is used to hold each tungsten lead-in wire in position with respect to the rack. We try to have as small a contact of the tungsten lead-in with the rack as possible so that we won't have any noise (spurious reflections) caused by the rack. The rack with wires is described in Fig. 8.

Each specimen is welded to a lead-in line of tungsten which is terminated outside the glass tube by a magnetostrictive Remendur stub. The lines are driven by Panametrics' magnetostrictive transducer Model KT-55 and Panametrics' Panatherm^(R) Model 5010, and monitored with a Tektronix 535 oscilloscope.

In the whole experiment, we keep the vacuum below 90 micron in order to minimize the oxidation of the samples and lead-in.

C. Measurements on Remendur to 1000°C

1. Samples

Several samples of Remendur wire have been measured. We are reporting on two of them.

The dimensions of Sample 3 and Sample 4 are given in Table IV. The lead-in wires are tungsten of 0.1 cm in diameter.

Table IV

Sample	Diameter	Length
3	0.075 cm	7.04 cm
4	0.075 cm	9.32 cm

Samples 3 and 4 are simultaneously in the furnace through the measurements, Run 3 up, Run 4 up, and Run 4 down, for longitudinal modulus and attenuation. We find that both are functions of temperature in Figs. 9 through 12. A drastic change of curvature is seen around 600°C , which is half the melting point ($600\text{-}650^{\circ}\text{C}$) for Remendur wire. This agrees with similar data for other alloys.⁹

2. Run 3, Temperature Increasing, Modulus Data

For Run 3 we heated the samples from room temperature to 920°C and drove the two samples with magnetostrictive transducers of the same frequency (140 kHz). The modulus data are shown in Figs. 9 and 10 with square symbols for the data points. For longitudinal modulus, we find the two curves are of the same shape and the difference in value is within our experimental errors.

3. Run 4, Temperature Increasing, Modulus Data

In this experiment, we cut the length of the transducer stub for Sample 3 to less than half of its original length to make the frequency of the driven pulse 200 kHz, but for Sample 4 we keep the same frequency (140 kHz). Temperatures are from room temperature to 927°C and data points are circles. The two curves for modulus are of the same shape and the difference is within experimental errors.

4. Run 4, Temperature Decreasing, Modulus Data

The measurements are taken as the temperature in Run 4 returned to room temperature. In comparing the two curves for Sample 4 and Sample 3, we find 3 percent difference between the two. In comparing Run 4 down with Run 4 up for each sample, we find that for Sample 4 they go almost the same curve except the hysteresis, in the range $500\text{--}900^{\circ}\text{C}$. However, for Sample 3 the difference between Run 4 up and Run 4 down is evident and difference is up to 4 percent at temperatures below 500°C . We suspect that this difference is caused by the changing of the length of

the transducer stub of the Remendur for Sample 3. Further experiments are planned to study this. If this is true, the longitudinal modulus is a function of frequency as well as temperature.

5. Reflection Coefficient

For reflection coefficient, we found it to be around 60% through all the experiments.

6. Attenuation

In general, attenuation began to increase drastically above half the melting point absolute. See Figs. 11 and 12. At lower temperatures, we find many negative points as shown in Fig. 11, but when we calculate the maximum errors, we find that our maximum error can be very big with respect to small values of α . (The calculation is in III C.) Reasonable curves can be drawn if the maximum errors are considered. We found that α is the same (within experimental errors) below 500°C for all the runs with both samples except for Run 4 down with Sample 4. For Sample 4, the curve we get for Run 4 down is strange; we do not know the reason yet.

D. Statistical Errors in Attenuation and Reflection Coefficient

In the pulse-echo technique with a lead-in line, to determine reflection coefficient and attenuation coefficient we use the amplitudes of echoes. the interface echo A and two free back echoes, B and C. Appropriate formula has been derived by E. P. Papadakis^{10,11}

$$R = [\bar{A}\bar{C}/(\bar{A}\bar{C} - 1)]^{1/2}$$

$$\alpha = [\ln(R/\bar{C})] / 2L$$

where $\bar{A} = \frac{A}{B}$ $\bar{B} = \frac{C}{B}$

In measuring the A, B, and C echoes, our errors can be $\pm 1\%$, so, when error is taken into consideration

$$A \longrightarrow A(1 \pm \delta) \quad B \longrightarrow B(1 \pm \delta) \quad C \longrightarrow C(1 \pm \delta)$$

where $\delta = 0.01$

$$\bar{A} = \frac{A (1 \pm \delta)}{B (1 \pm \delta)} = \frac{A}{B} (1 \pm 2 \delta) = \frac{A}{B} (1 \pm \epsilon) \dots \quad (17)$$

$$\bar{C} = \frac{C (1 \pm \delta)}{B (1 \pm \delta)} = \frac{C}{B} (1 \pm 2 \delta) = \frac{C}{B} (1 \pm \epsilon) \dots \quad (18)$$

where $\epsilon = 0.02$

$$\begin{aligned} \left\{ R = \frac{\bar{A} \bar{C}}{\bar{A} \bar{C} - 1} \right\}^{1/2} &\Rightarrow \left\{ \frac{\bar{A} (1 \pm \epsilon) \bar{C} (1 \pm \epsilon)}{\bar{A} (1 \pm \epsilon) \bar{C} (1 \pm \epsilon) - 1} \right\}^{1/2} \\ &= \left\{ \frac{\bar{A} \bar{C} (1 \pm 2 \epsilon)}{\bar{A} \bar{C} (1 \pm 2 \epsilon) - 1} \right\}^{1/2} \\ &= \left\{ \frac{\bar{A} \bar{C} (1 \pm 2 \epsilon)}{(\bar{A} \bar{C} - 1) \left[1 \pm \frac{2 \epsilon \bar{A} \bar{C}}{\bar{A} \bar{C} - 1} \right]} \right\}^{1/2} \\ &= \left\{ \frac{\bar{A} \bar{C}}{\bar{A} \bar{C} - 1} \left[1 \pm 2 \epsilon \mp \frac{2 \epsilon \bar{A} \bar{C}}{\bar{A} \bar{C} - 1} \right] \right\}^{1/2} \\ &= R \left\{ 1 \pm 2 \epsilon (1 - R^2) \right\}^{1/2} \\ &\approx R \left\{ 1 \pm \epsilon (1 - R^2) \right\} \end{aligned} \quad (19)$$

so the maximum error in R is

$$\frac{\Delta R_{\max}}{R} = \epsilon (1 - R^2) \leq 0.02 \dots \quad (20)$$

The statistical deviation is calculated for α as follows:

$$\alpha = \frac{\ln(-\frac{R}{\bar{C}})}{2L} \quad \text{the } R \text{ and } \bar{C} \text{ are different in sign}$$

$$2\alpha L = \ln(-\frac{R}{\bar{C}})$$

$$e^{2\alpha L} = (-\frac{R}{\bar{C}})$$

$$\ln(e^{2\alpha L}) = \ln(-\frac{R}{\bar{C}}) = \ln R - \ln \bar{C}$$

$$\frac{d(e^{2\alpha L})}{e^{2\alpha L}} = \frac{dR}{R} - \frac{d\bar{C}}{\bar{C}}$$

From (18) and (20),

$$\left| \frac{\Delta(e^{2\alpha L})}{e^{2\alpha L}} \right| = \left| \frac{\Delta R}{R} \right| + \left| \frac{\Delta \bar{C}}{\bar{C}} \right| \leq \epsilon + \epsilon = 0.04 \text{ ---} \quad (21)$$

$\Delta(e^{2\alpha L})$ can be expressed by use of the differentiation formula

$$\frac{d}{du}(e^u) = e^u$$

$$d(e^u) = e^u du$$

$$\Delta(e^u) = e^u \Delta u$$

$$\Delta(e^{2\alpha L}) = e^{2\alpha L} \Delta(2\alpha L)$$

so Eq. (21) reduces to

$$\Delta(2\alpha L) = \left| \frac{\Delta R}{R} \right| + \left| \frac{\Delta \bar{C}}{\bar{C}} \right| \leq 2\epsilon = 0.04 \quad (22)$$

Since L is held constant,

$$\Delta \alpha \approx \frac{0.02}{L} \quad (23)$$

Using the dimensions in Table IV, in Sample 3 $\Delta \alpha \approx 0.003$, and $\alpha \approx 10^{-4}$ at temperature below 500°C , so percentage error can be 3000%. That is the reason that α comes out to be negative, but when the deviation is taken into consideration we can draw a reasonable curve with $\alpha \approx 0$. (There is also a curve of percentage error¹¹ in R and $2 \alpha L$ with respect to R in Fig. 13.)

IV. PUBLICATIONS, TALKS, COURSES, COMMITTEES, STUDENTS

A. Papers Published

The following papers on work supported wholly or in part by ONR have been published:

E. P. Papadakis, "On the Absolute Accuracy of the Pulse-Echo-Overlap Method and the Pulse-Superposition Method for Ultrasonic Velocity," J. Acoust. Soc. Amer. 52, 843-846 (1972).

E. P. Papadakis, "Ultrasonic Diffraction Loss and Phase Change for Broadband Pulses," J. Acoust. Soc. Amer. 52, 847-849 (1972).

E. P. Papadakis, L. C. Lynnworth, K. A. Fowler, and E. H. Carnevale, "Ultrasonic Attenuation and Velocity in Hot Specimens by the Momentary Contact Method With Pressure Coupling, and Some Results on Steel to 1200C," J. Acoust. Soc. Amer. 52, 850-857 (1972).

E. P. Papadakis, "Tabulation of the Coefficients of a Quadratic Function for the Thermal Expansion of Various Alloys and Other Engineering Materials," Materials Science and Engineering 10, 195-203 (1972).

E. P. Papadakis, K. A. Fowler, and L. C. Lynnworth, "New Uses for Ultrasonic Spectrum Analysis," Proc. 1972 IEEE Ultrasonics Symposium, IEEE #72 CHO 708-8 SU, IEEE, 345 E 47 St., N. Y., N. Y. 10017, 1972, pp. 81-86.

L. C. Lynnworth, "Torsional Wave Transduction in Magnetostrictive Wire," Ultrasonics 10, (5), 195-197 (Sept. 1972).

L. C. Lynnworth, "High Temperature Measurements," Research/Development 23, (10), 8 (Oct. 1972). Note: Over 100 responses were received concerning this Letter to the Editor.

B. Papers Scheduled

The following papers on work supported wholly or in part by ONR are scheduled for publication in the near future:

L. C. Lynnworth, E. P. Papadakis, and K. A. Fowler, "Ultrasound Propagation Measurements and Applications," Proc. ARPA-AMMRC Symposium on Advanced NDT Techniques (to be published).

K. A. Fowler, "Ultrasonic Transducer Characterization," Proc. ARPA-AMMRC Symposium on Advanced NDT Techniques (to be published).

L. C. Lynnworth and E. H. Carnevale, "Ultrasonic Thermometry Using Pulse-Echo Techniques," Proc. 5th Symposium on Temperature-Its Measurement and Control in Science and Industry (to be published).

L. C. Lynnworth, "Attenuation Measurements Using the Pulse-Echo AB Method," Materials Evaluation (to be published).

E. P. Papadakis, K. A. Fowler, and L. C. Lynnworth, "Ultrasonic Attenuation by Spectrum Analysis of Pulses in Buffer Rods: Method and Diffraction Corrections," J. Acoust. Soc. Amer. (to be published).

E. P. Papadakis, "Lens Equation for Focused Transducers," International Journal of Nondestructive Testing (to be published).

E. P. Papadakis, "Balanced Resonator for Infrasonic Measurements of Young's Modulus and Damping in Flexure," ASTM J. Testing and Evaluation (to be published).

L. C. Lynnworth, "Ultrasonic Measurement of Elastic Moduli in Slender Specimens Using Extensional and Torsional Wave Pulses," ASTM J. Testing and Evaluation (to be published).

E. P. Papadakis, "Measurement of Small Changes in Ultrasonic Velocity and Attenuation," (Invited) Crit. Rev. Solid State Sciences (to be published).

E. P. Papadakis, "Ultrasonic Diffraction From Single Apertures," Physical Acoustics, Principles and Methods, W. P. Mason and R. N. Thurston, Eds., Academic Press, N. Y. (future volume to be published).

C. Talks Given

The following talks on work supported wholly or in part by ONR were given recently:

E. P. Papadakis, "Ultrasonic Methods for Modulus Measurement in Paper," TAPPI Testing Conference, Philadelphia, Pa., Sept. 26-29, 1972.

E. P. Papadakis, K. A. Fowler, and L. C. Lynnworth, "New Uses for Ultrasonic Spectrum Analysis," IEEE Ultrasonics Symposium, Boston, Mass., Oct. 3-7, 1972.

C. A. Carey, "Sound Propagation in High-Temperature Plasmas," IEEE Ultrasonics Symposium, Boston, Mass., Oct. 3-7, 1972.

L. C. Lynnworth and N. E. Pedersen, "Ultrasonic Mass Flowmeter," IEEE Ultrasonics Symposium, Boston, Mass., Oct. 3-7, 1972.

D. Talks Scheduled

The following talks on work supported wholly or in part by ONR are scheduled for the near future:

L. C. Lynnworth, "Ultrasonic Temp. Profiling and Attenuation," ASTM-E20.06, Washington, D. C. (Nov. 17, 1972).

L. C. Lynnworth, "Nuclear Reactor Applications of Ultrasound," IEEE Boston Section, Joint Meeting of Groups on Nuclear Science and on Sonics/Ultrasonics (Feb. 5, 1973).

E. Professional Societies

L. C. Lynnworth is secretary of ASTM Subcommittee E-20.06, Acoustical Thermometry. He is also chairman of the Boston Section of the IEEE Group on Sonics and Ultrasonics. E. P. Papadakis is Editor of the Newsletter and Associate Editor for industrial ultrasonics of the Transactions on Sonics and Ultrasonics of the IEEE Group on Sonics and Ultrasonics with about 1200 members. He is also serving on the Physical Acoustics committee of the Acoustical Society of America, on the Working Group on Ultrasonic Attenuation and Velocity (E-07.06.13) of ASTM Subcommittee E-07.06, on ASTM Subcommittee D-20.15 concerned with Dynamic Properties of Plastics, on an ad-hoc committee for improved nondestructive testing methods under the auspices of the National Science Foundation and the Air Force Materials Laboratory, and on the independent Acoustic Emission Working Group. K. A. Fowler is also serving on the latter group.

F. Students

James Chen, a graduate student in the Physics Dept. at Boston College, is working at Panametrics on this research. It is anticipated that he will find a doctoral thesis topic within the scope of the work under this contract.

G. Course

Our course #2911 Ultrasonics, will be offered again at the Northeastern University Extension School when sufficient interest has been shown to warrant it in the judgment of the University administration.

REFERENCES

1. L. C. Lynnworth, E. H. Carnevale, and D. R. Patch, "Ultrasonic Profile Measuring Apparatus," U.S. Patent No. 3,636,754 (Jan. 25, 1972).
2. L. C. Lynnworth, "Dual Ultrasonic Sensors Employing a Single Mode of Ultrasonic Transmission," U.S. Patent No. 3,580,058 (Aug. 1970).
3. L. C. Lynnworth, "Dual Ultrasonic Sensors Employing Differing Modes of Ultrasonic Transmission," U.S. Patent No. 3,540,265 (May 1968).
4. E. P. Papadakis, J. Appl. Phys. 42 (7) 2990-2995 (June 1971).
5. L. C. Lynnworth and B. J. Spencer, "Magnetostrictive Ultrasonic Transducer," U.S. Patent No. 3,633,424 (Jan. 11, 1972).
6. L. C. Lynnworth, "High Temperature Ultrasonic Measuring System," U.S. Patent No. 3,538,750 (Nov. 10, 1970).
7. L. C. Lynnworth and B. J. Spencer, "Ultrasonic Sensing System," U.S. Patent No. 3,514,747 (May 26, 1970).
8. L. C. Lynnworth, et al., IEEE Trans. Nucl. Sci. NS-18 (1) (Feb. 1971).
9. Annual Summary Report, ONR Contract N00014-71-C-0050, (Aug. 15, 1971) p. 18.
10. E. P. Papadakis, L. C. Lynnworth, K. A. Fowler, and E. H. Carnevale, J. Acoust. Soc. Amer. 52, 850-857 (1972).
11. E. P. Papadakis, J. Acoust. Soc. Amer. 44, 1437-1441 (1968).

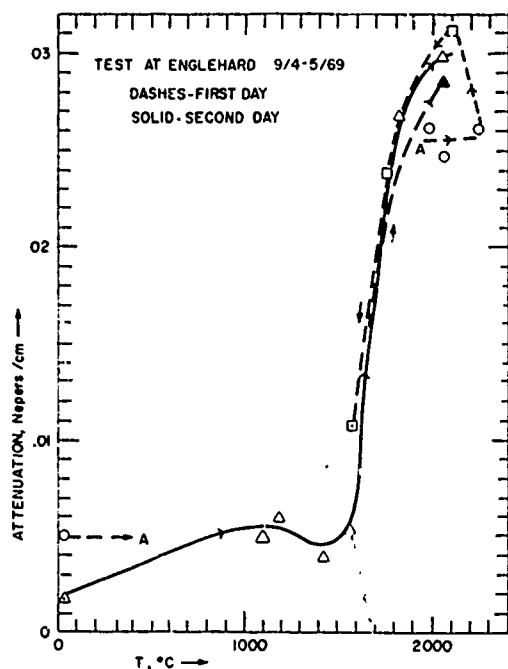


Fig. 1. Attenuation in a rhenium sensor when broad band echoes of about 100-kHz center frequency were used and when the reflection coefficient and the attenuation were computed simultaneously from three echo amplitudes.⁴ After the first day's initial heating to 2240°C , the attenuation assumed a fairly steady functional dependence upon temperature.

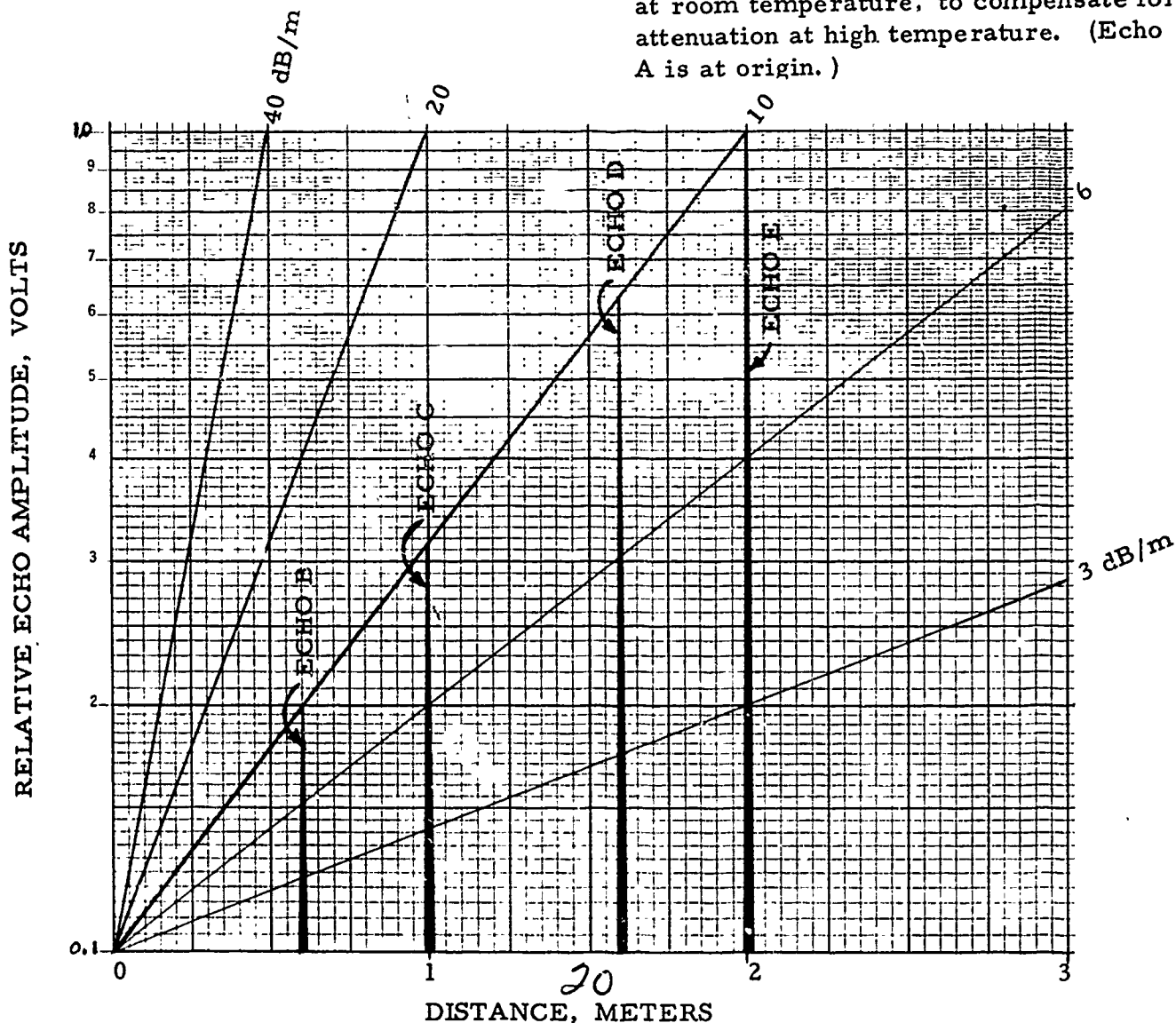


Fig. 2. Determination of echo amplitudes at room temperature, to compensate for attenuation at high temperature. (Echo A is at origin.)

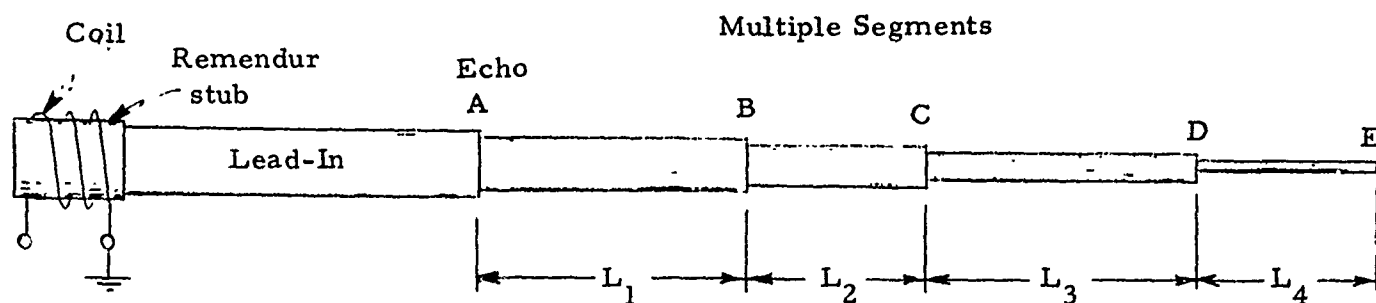


Fig. 3. Line containing four sensing segments: $L_1 = L_3 = 60$ cm, $L_2 = L_4 = 40$ cm. Lead-in and segments are all of one material. Diameter steps are designed to provide echoes large enough at room temperature to compensate for attenuation at high temperature. Lengths L_i are staggered to avoid echo interferences at room temperature.

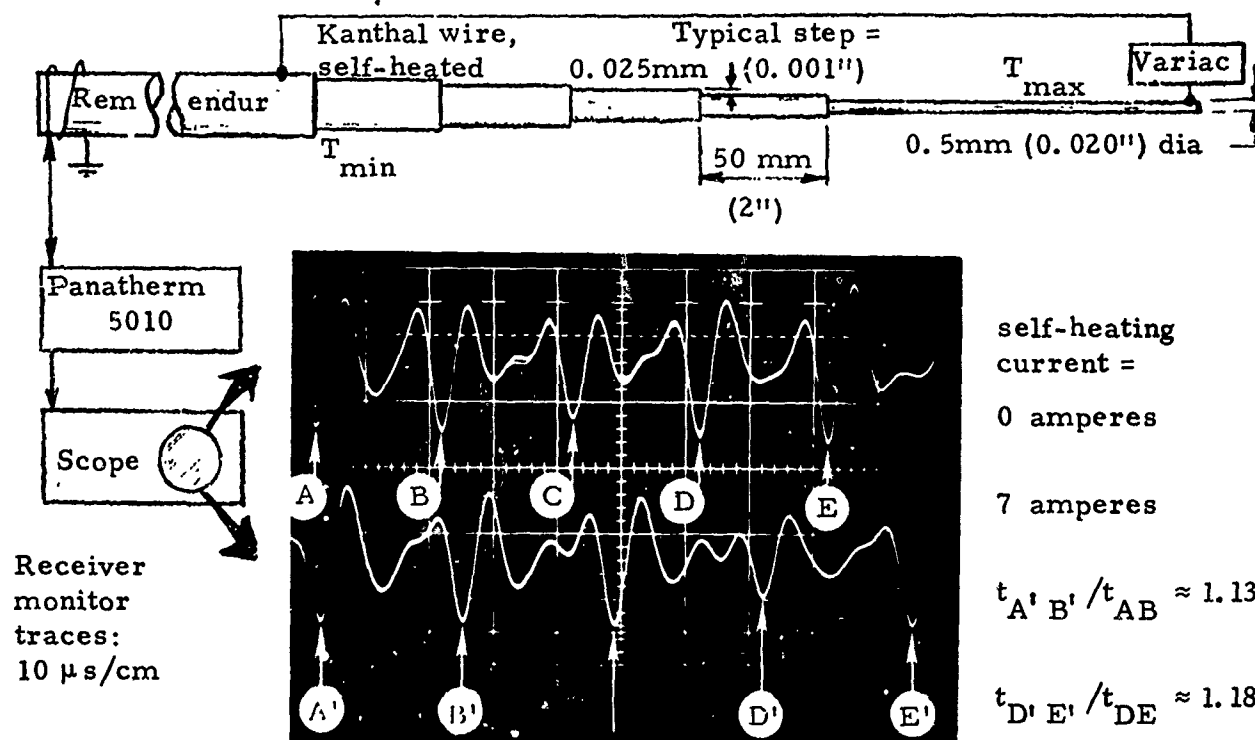
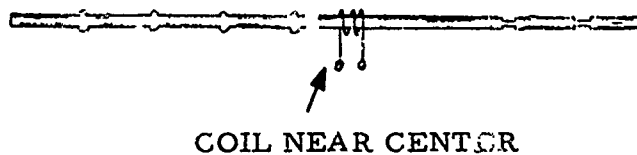
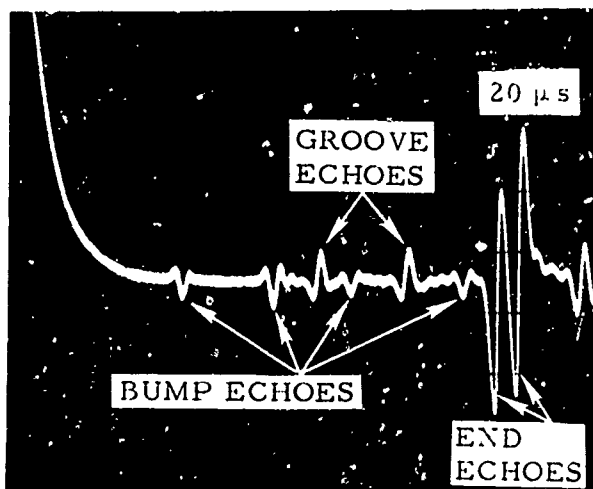
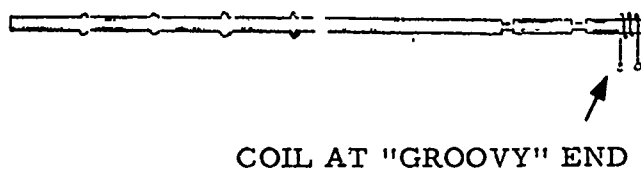
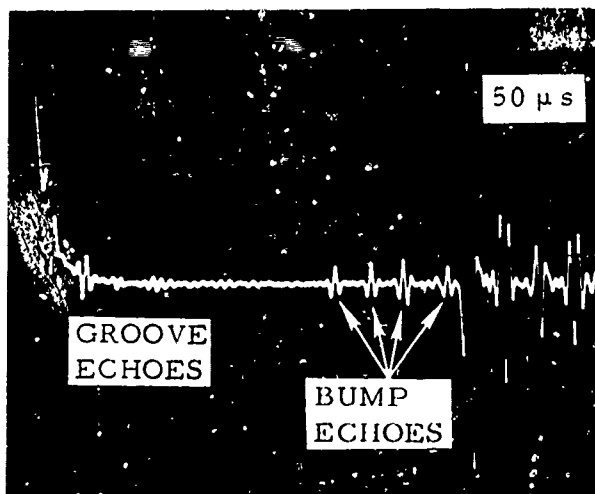
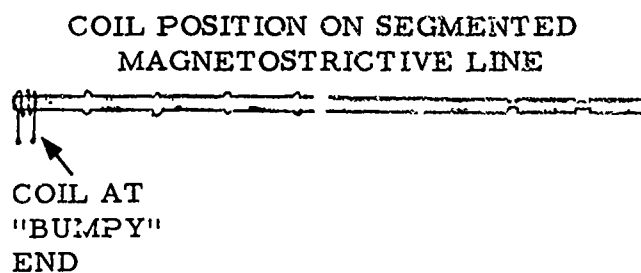
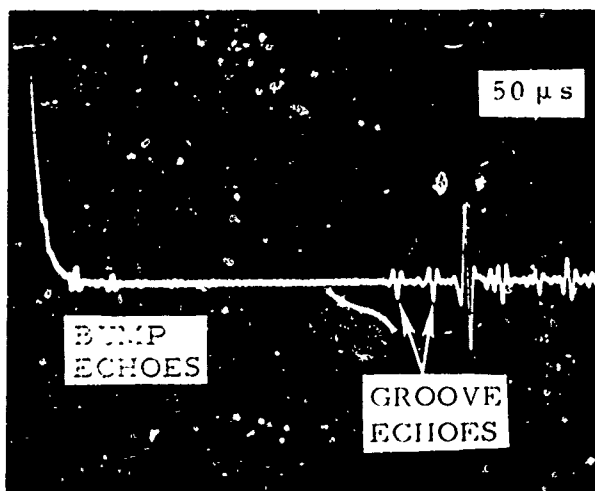
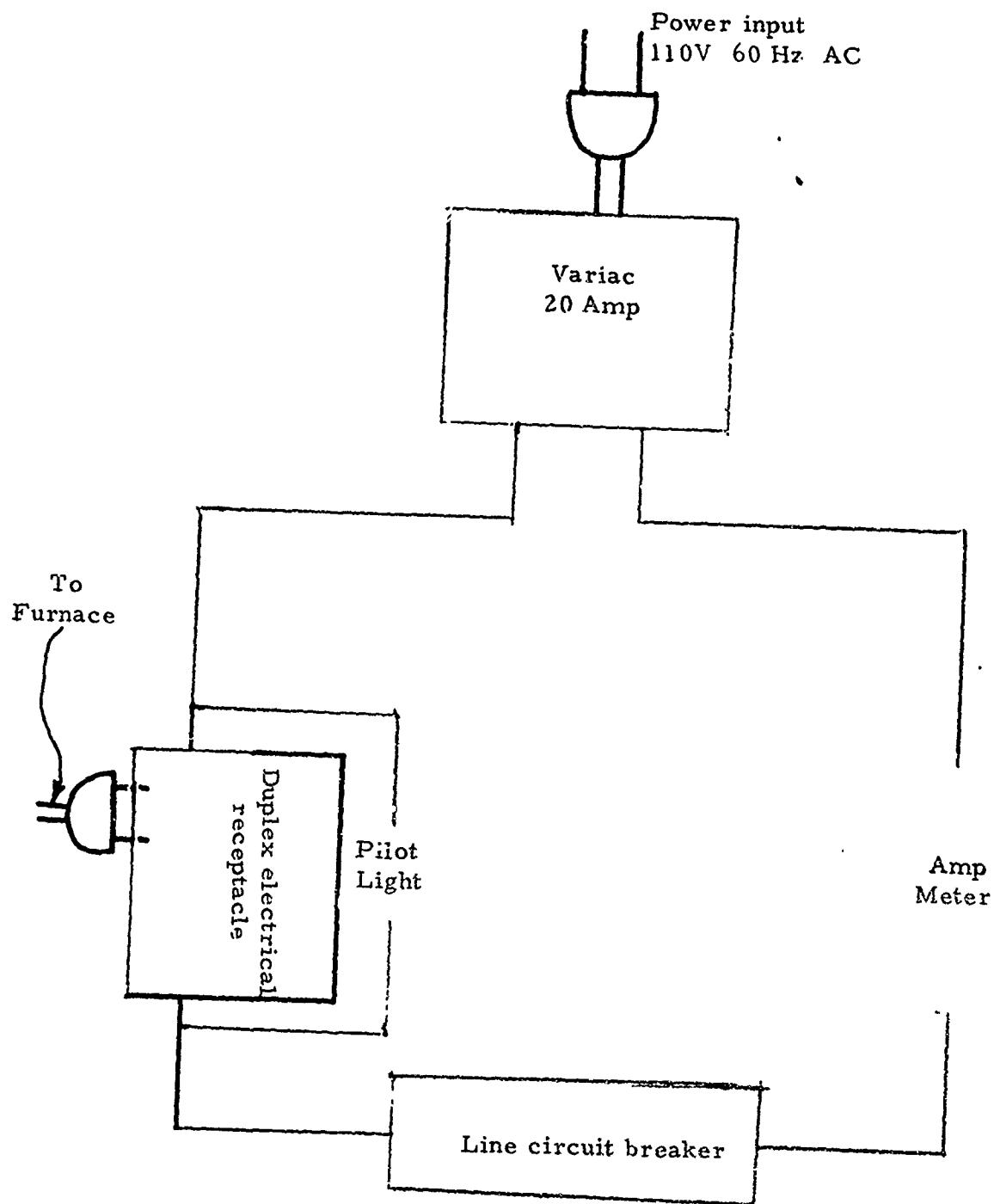


Fig. 4. Echo response to thermal gradient. Echoes obtained from a Kanthal wire containing series sensors of monotonically decreasing diameter. Stepped-diameter wire, when electrically self-heated, illustrates profiling.⁸



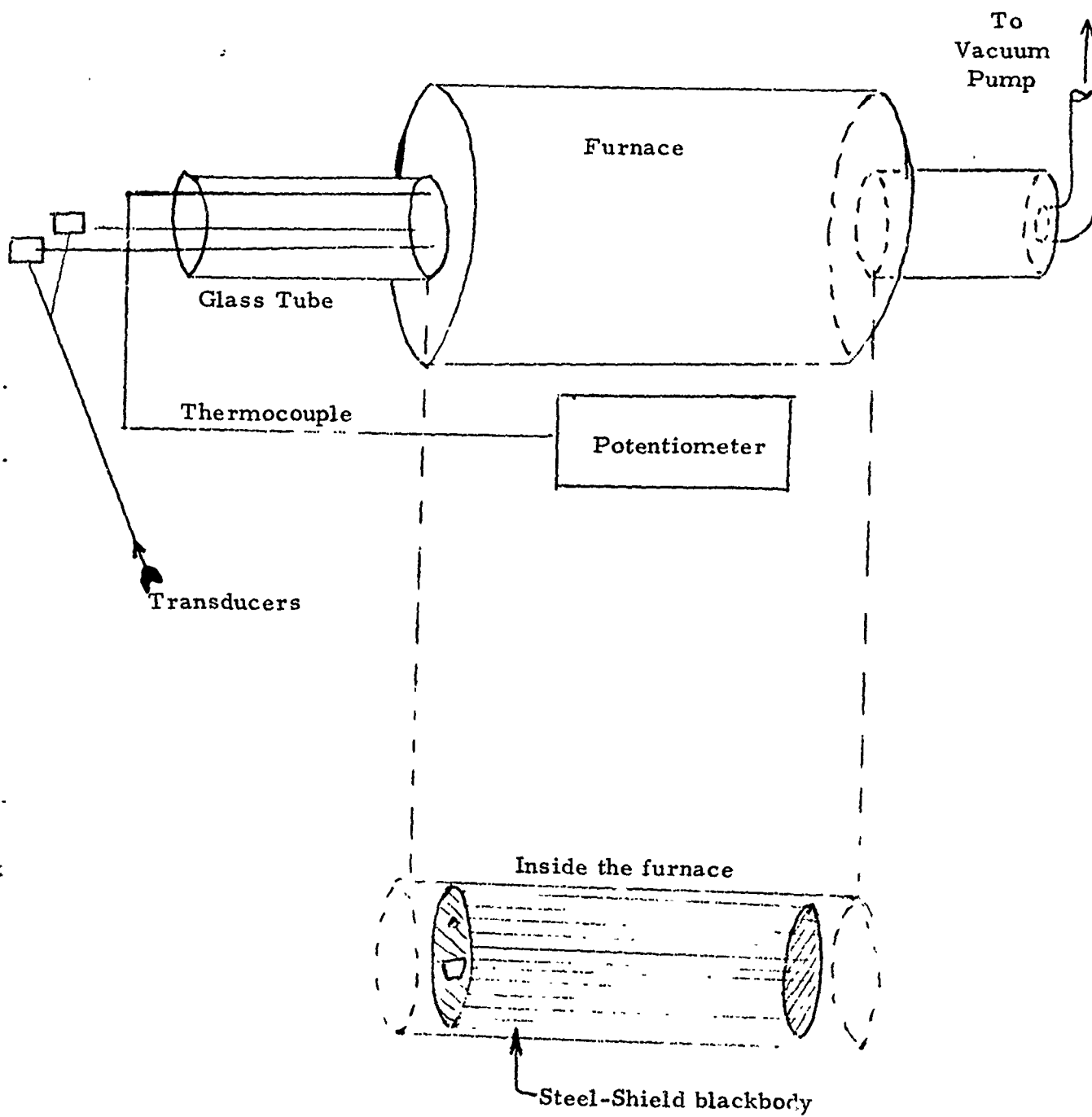
22

Fig. 5. Test configuration and oscillograms



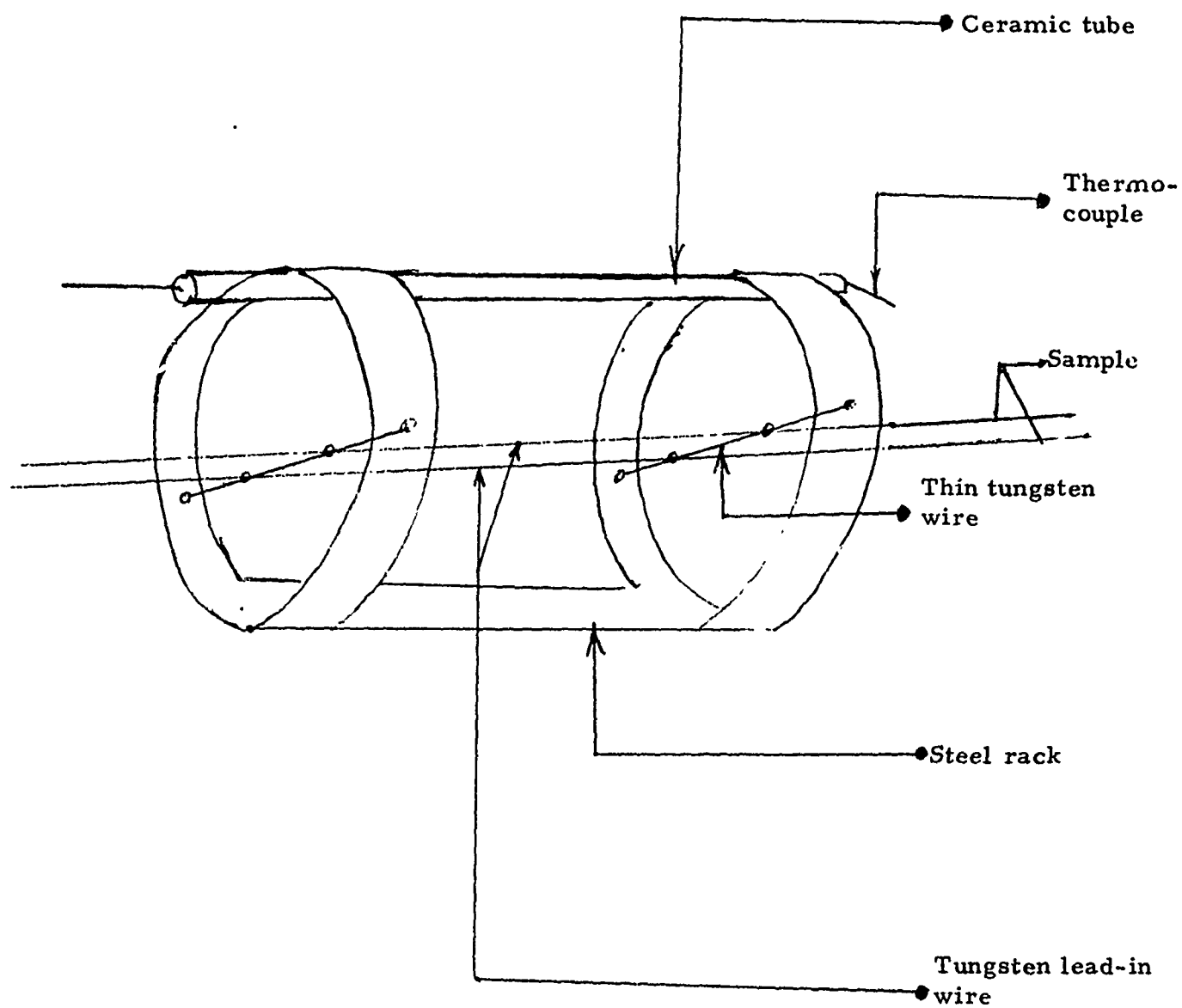
23

Fig. 6. Electrical heater control console.



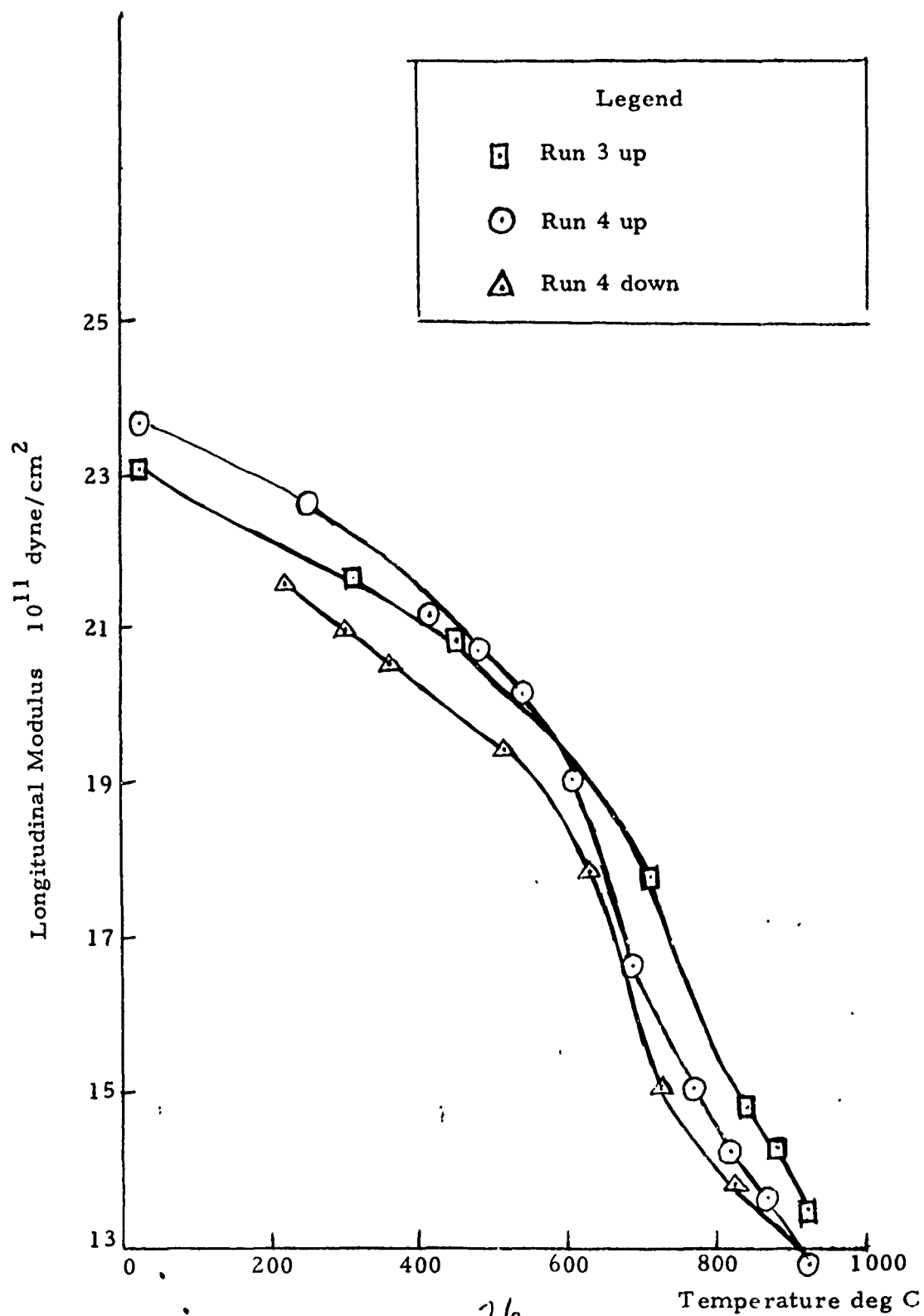
24

Fig. 7. 1000°C furnace configuration.

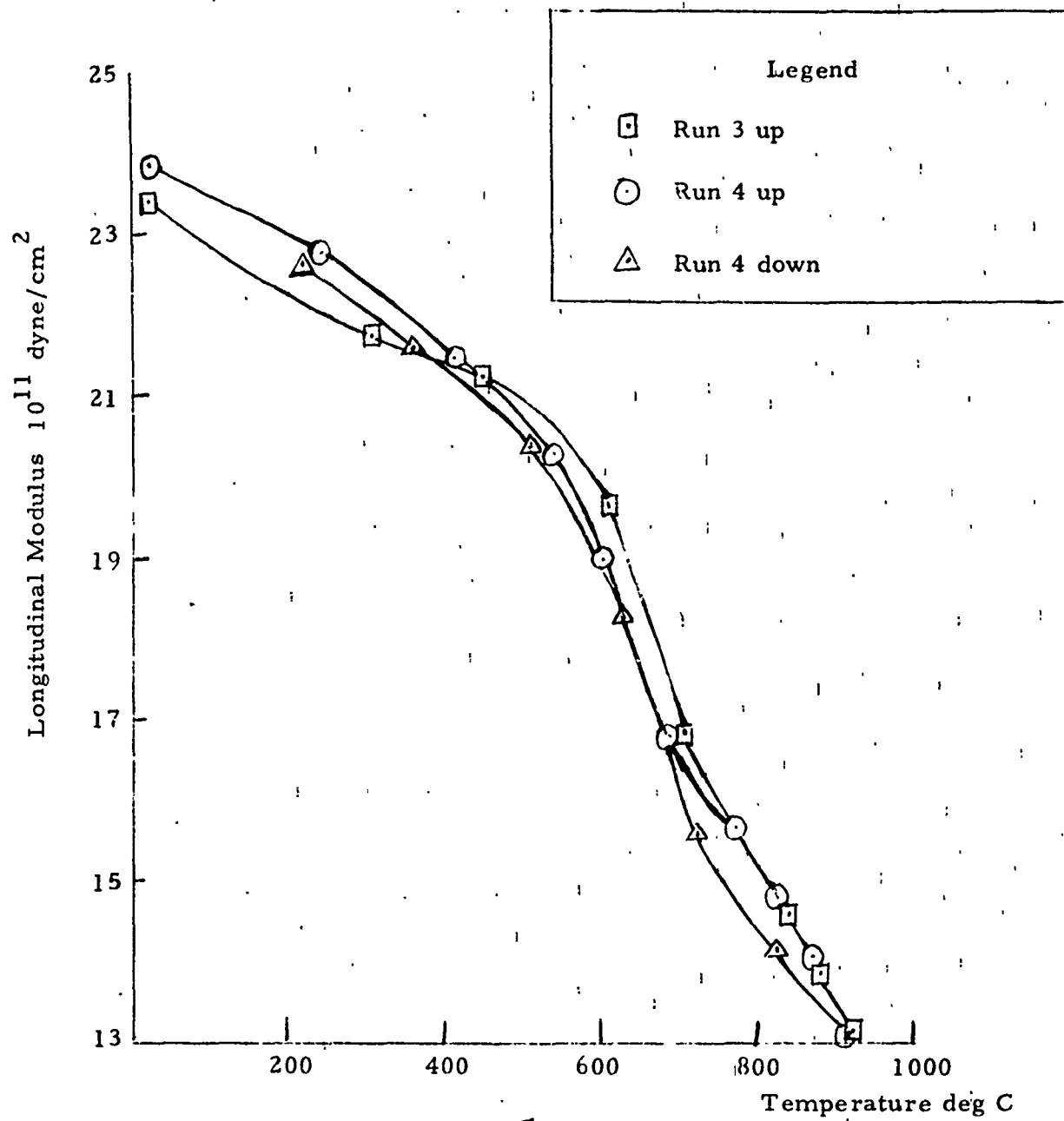


25

Fig. 8. Rack configuration for holding lead-in wires and thermocouple.



26
Fig. 9. Longitudinal wave modulus in remendur wire for sample 3.



27
Fig.10. Longitudinal modulus in remendur wire for sample 4.

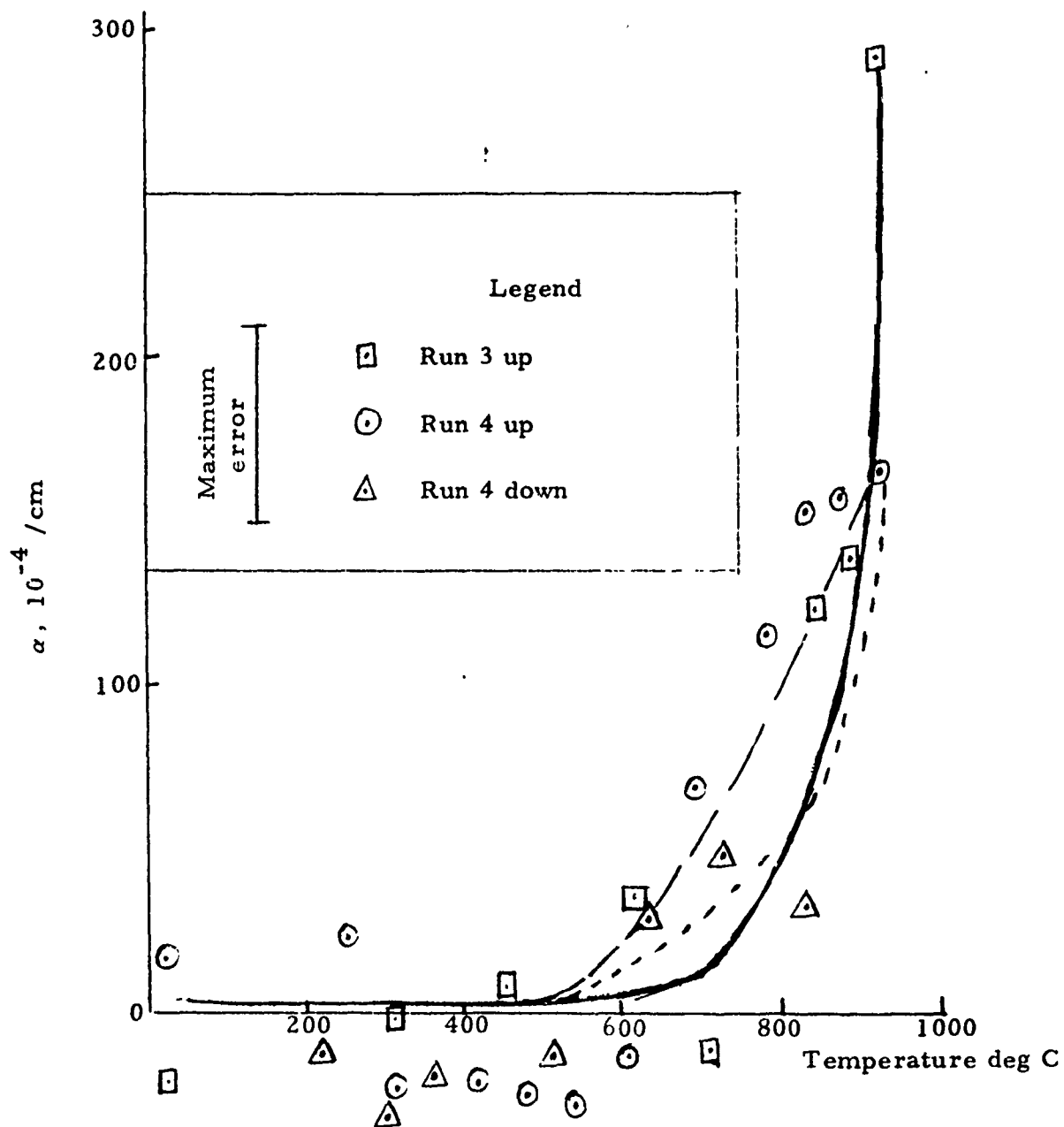
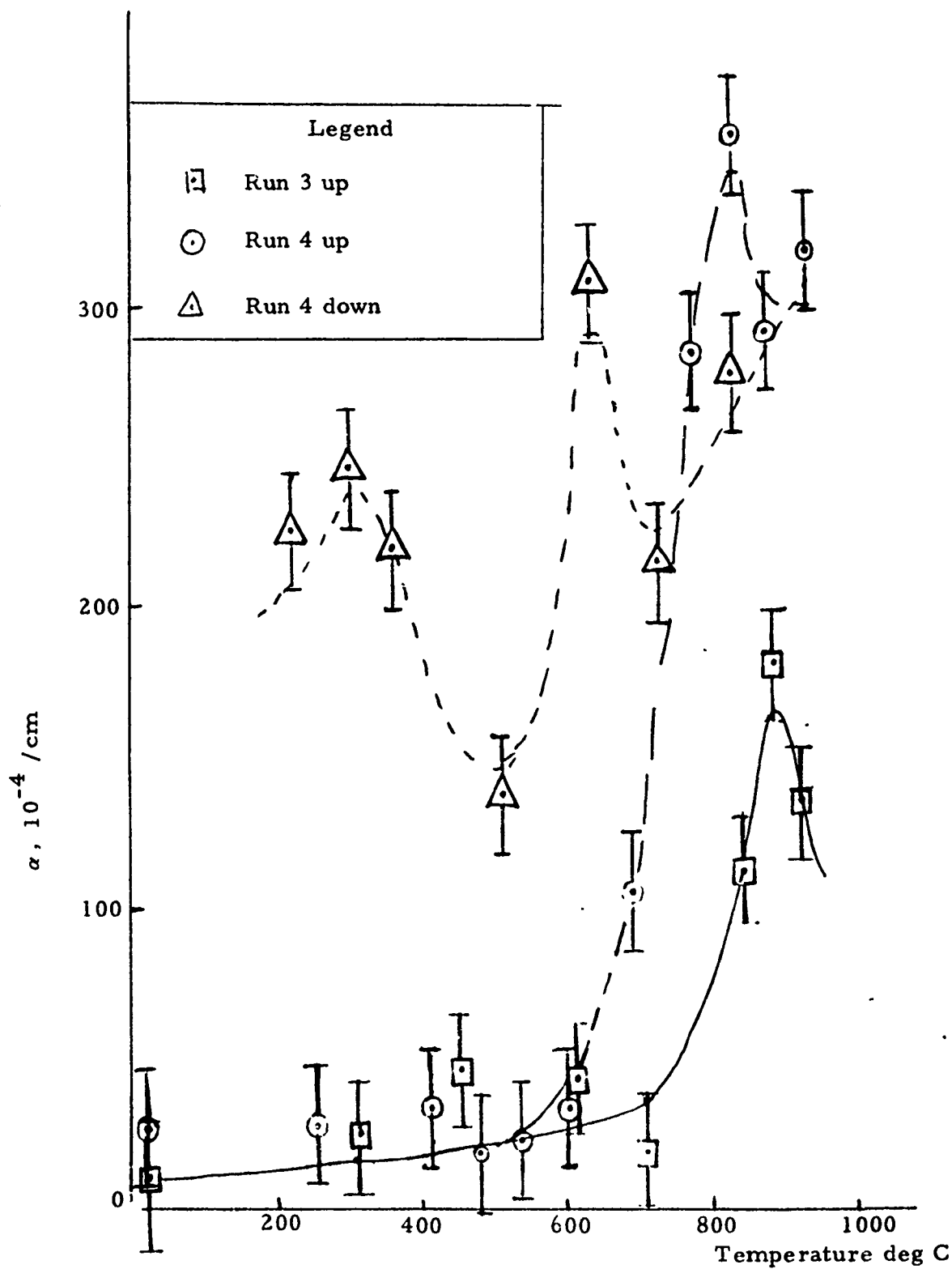


Fig. 11. Attenuation coefficient for sample 3.



29

Fig. 12. Attenuation coefficient for sample 4.

1/7
APPENDIX A



PANAMETRICS

221 Crescent Street • Waltham, Massachusetts 02154 • (617) 899-2719

MONITORING THE MODULI OF POLYMERS
WITH ULTRASOUND

by

Emmanuel P. Papadakis

ABSTRACT

Two ultrasonic methods are presented for the measurement and monitoring of the elastic moduli of polymers and other liquids undergoing solidification. The methods are thought to be most sensitive to the build-up of the real component of the modulus of rigidity of the material. Ultrasonic traveling waves are used to interrogate a boundary between the solid body transmitting the wave and the sample under test. Data on epoxy resins are given.

I. INTRODUCTION

The behaviour of epoxy resins during hardening was studied as a function of time by means of ultrasonics. Both bulk wave and wire wave methods were employed, and were found to complement each other. The propagation media (glass blocks and tungsten wires) were partially immersed in beakers of epoxy, and the increasing energy transfer into the epoxy noted as it hardened. Temperature was monitored simultaneously. Quantitative results were obtained, but their interpretation is complicated by two factors:

- 1) The exothermic nature of the polymerization and cross-linking reactions which raised the temperature in the epoxy, and
- 2) The fact that the glass transition temperature rises during polymerization, being below the epoxy temperature at the start of polymerization and above the epoxy temperature after curing. (1, 2)

The methods, however, hold promise for further study of polymers and plastics.

II. EXPERIMENTS WITH BULK WAVES

A glass buffer rod with plane parallel ends having an ultrasonic transducer bonded to one end was inserted into a pot of epoxy mixed with hardener as shown in Fig. 1. Echoes within the rod were observed on an oscilloscope and recorded photographically during the curing process. The temperature of the epoxy was monitored by a thermocouple, and is plotted as a function of log (time) in Fig. 2, along with the temperature of the curing oven. The portion of the wave entering the epoxy did not return to the sample because of attenuation in the epoxy and diffusion at

the uneven surface of the pot. Thus the amplitudes of the first and second echoes in the glass sample give the reflection coefficient between the glass and the epoxy as

$$R = \frac{A_2/A_1}{(A_2/A_1)_0} \quad (1)$$

where the denominator with the subscript $_0$ is the amplitude ratio before the sample is dipped into the pot of epoxy. This normalization takes care of attenuation and beam spreading in the buffer rod. R is related to the mechanical impedances of the glass Z_G and epoxy Z_E by the formula⁽³⁾

$$R = \frac{Z_G - Z_E}{Z_G + Z_E} \quad (2)$$

which can be solved for the unknown Z_E as follows:

$$Z_E = Z_G \frac{1-R}{1+R} \quad (3)$$

Z_E is found as a function of time by recording A_1 and A_2 as functions of time. Since density ρ remains almost constant during the reaction, and since⁽⁴⁾ $Z = \rho v$ where v is the ultrasonic velocity, Z is essentially a measure of v . Since⁽⁵⁾ $v = (M/\rho)^{1/2}$ where M is the appropriate modulus of elasticity for the wave motion, Z_E is really a measure of $(M)^{1/2}$ as it exists in the epoxy at any instant.

DER 332 epoxy resin* and MPDA hardener mixed 6.5:1 by weight were used in this experiment with 5 MHz ultrasonic waves, both shear and longitudinal. The cure was effected in an oven held at $61 \pm 1^\circ \text{C}$. The data on the reflection coefficients versus time are plotted in Fig. 3. In the longitudinal case, the reflection coefficient dropped from an initial value of 0.77 at the glass-liquid interface to a final value of 0.620 at the glass-cured solid interface. The time for half the change to occur was

*Dow Epoxy Resin, type 332

200 min. In the shear wave case, R dropped from an initial value of 0.990 to a final value of 0.715 with a half-life of 170 min. The difference in curing times is due to differences in time and temperature during mixing and outgassing the mixtures of resin and hardener before applying them to the ultrasonic samples.

One notices that the change in reflectivity occurs in a precipitous and symmetrical manner about the time of half-hardness when plotted on semilogarithmic paper in Fig. 3. These data were used to compute Z_E from Eq. (3). The relative change of Z_E with time is shown in Fig. 4. The growth is very rapid about $t_{1/2}$. The limiting values of Z_E are given in Table I in terms of the impedance of the glass found from measured values of $\rho = 2.21 \text{ g/cm}^3$, $v_l = 5.61 \times 10^5 \text{ cm/sec}$, and $v_s = 3.44 \times 10^5 \text{ cm/sec}$.

Table I
Impedances of DER 332 at 61°C in $10^{11} \text{ gm cm}^{-2} \text{ sec}^{-1}$.

Wave	Mixed		Cured	
	Z_E/Z_G	Z_E	Z_E/Z_G	Z_E
Longitudinal	0.123	1.52	0.237	2.94
Shear	0.005	0.038	0.166	1.26

III. EXPERIMENTS WITH WIRE WAVES

Three experiments were performed with ultrasonic waves in wires to test single-ended wire delay lines as monitors for polymerization. In these cases, the wavelength is much larger than the wire diameter, so longitudinal waves travel in the long wavelength extensional wave limit, and torsional waves travel in a single mode. All three experiments utilized the same electronic system, a Panatherm 5010^(R) ultrasonic thermometer

instrument with a magnetostrictive transducer, a wire delay line, and a monitoring oscilloscope. See the block diagram in Fig. 5. The Panatherm pulses the transducer coil repetitively with a current spike, generating stress pulses in the lead-in wire. These pulses echo from both ends of a sensor welded to the end of the lead-in wire, and yield echoes seen in Fig. 6. The Panatherm measures the time between selected pairs of echoes, and the amplitude of these echoes. The amplitudes may also be photographed on the monitoring oscilloscope, as done in these experiments. From the travel time between echoes, and the length of the sensor, one can compute the velocity in the sensor material. With a calibrated sensor (travel time versus temperature) the instrument is an ultrasonic thermometer. From the amplitudes of the first three echoes, one may compute⁽⁶⁾ the attenuation in the sensor and the reflection coefficient at the lead-in/sensor weld.

In one experiment, the sensor was immersed vertically in a vial of epoxy such that the meniscus coincided with the lead-in/sensor weld. The purpose was to measure the attenuation in the wire as the epoxy became more viscous and then hardened, and so to monitor changes in the epoxy. The echoes were photographed from the oscilloscope and the temperature of the epoxy was monitored with a thermocouple. A Joule-Wiedemann transducer⁽⁷⁾ was employed, giving both extensional and torsional waves. Reflection coefficients and attenuation were computed, and are shown in Fig. 7. It can be seen that the rapid rise in attenuation coincides with the rapid rise in temperature due to the exothermic reaction, and that in a matter of minutes the attenuation becomes too large to measure. The attenuation can arise from viscous damping as the viscosity increases, and from radiation as the real part of the modulus in the epoxy grows.

In a second experiment, a lead-in wire with no sensor attached was immersed to a length of about 10 cm in a vial of epoxy which was cooled with tap water (8°C) in a surrounding coil. The purpose was to observe the echo

which was found to be generated at the meniscus when the epoxy begins to solidify. On solidification, the wire within the epoxy increases in effective acoustic impedance⁽⁴⁾ because of the adhering epoxy, and a definite echo is created at the meniscus. The amplitude of this echo was followed with oscilloscope photographs as the epoxy hardened. A plot is shown in Fig. 8. The echo becomes visible in less than 45 minutes, and grows slowly at this temperature until a rapid increase begins at about 200 minutes. The climb is interrupted at point A on the graph by an apparent partial disbonding between the wire and the epoxy. (Cracks were visible upon inspection after the experiment.) However, the echo amplitude continues to climb thereafter until another discontinuity appears at point B on the graph. It is thought that this, too, arose from partial disbonding. The echo at the meniscus is thought to be generated by the growth of the shear modulus (modulus of rigidity) of the epoxy.

A third experiment was performed to test the automatic capabilities of the Panatherm 5010 instrument to detect and record the initiation and growth of the echo at the meniscus of the epoxy. The system was set up as in Fig. 9 with the wire immersed to a depth $2L$ into a vial of epoxy. The first segment of length L was a sensor, while the second segment was part of the lead-in wire. The "Selector Monitor" of the Panatherm was set to observe the echoes from the weld (point II) and the end of the sensor (point III) while the echo from the meniscus was absent or small. The amplitudes A and B as measured by the Panatherm were sent to a multi-channel recorder. The trigger level in the Panatherm was set to cause the instrument to begin monitoring the echo at the meniscus (point I of Fig. 9) when it had grown to a small but finite value. The experiment when run resulted in data sketched schematically in Fig. 10 which represents the record on a strip chart. Initially the echoes from points II and III (charts A and B) fall as attenuation increases. When the echo from point I,

the meniscus, reaches the trigger level, the instrument jumps to monitor points I and II on charts A and B instead. The meniscus echo grows while the echo at point II continues to decrease in amplitude.

IV. DISCUSSION

Two ultrasonic methods have been presented for studying the growth of the elastic moduli of epoxy resins during polymerization. By extension, the methods could be used for other polymers and for liquids which change to a solid phase at a melting point or go through a glass transition. The two methods, using wire waves and bulk waves respectively, can operate from a few kHz to several GHz. The dividing line between them is in the range 500 kHz to 2 MHz, since bulk wave transducers for plane waves become excessively large below 500 kHz and since wire-sonic transmission lines become difficult to build above 2 MHz. The methods are applicable to the study of bulk quantities of liquids undergoing solidification. For thin layers, surface waves, Lamb waves and interface waves might be preferable, although the wire waves should be as sensitive. The methods react to relatively gross changes in system properties. For measuring smaller changes, see Ref. 8.

ACKNOWLEDGMENTS

The author is indebted to M. Lasky and R. Faires of ONR for continued support of this work. Conversations with E. H. Young and T. R. Meeker of Bell Telephone Laboratories, and with L. C. Lynnworth of this laboratory. proved valuable.

REFERENCES

1. N. Shito and M. Sato, J. Polymer Science: Part C 40, 1069-1078 (1967).
2. F. Nuayama and J. P. Bell, J. Polymer Science: Part A2 8, 437-445 (1970).
3. R. B. Lindsay, Mechanical Radiation, M Graw-Hill, N. Y., 1960, pp. 74-76.
4. R. B. Lindsay, op. cit., p. 218.
5. R. B. Lindsay, op. cit., p. 21.
6. E. P. Papadakis, J. Appl. Phys. 42, 2990-2995 (1971).
7. N. Tzannes, IEEE Trans. Sonics Ultrasonics 13, 33-41 (1966).
8. W. P. Mason, Physical Acoustics and the Properties of Solids, D. Van Nostrand, Princeton, N. J., 1958, pp. 107-113.

CAPTIONS

- Fig. 1. Block diagram of the experiment using ultrasonic bulk waves impinging upon epoxy resin at normal incidence.
- Fig. 2. Temperature in the oven and in the epoxy in experiment performed as in Fig. 1.
- Fig. 3. Reflection coefficients at the buffer/epoxy interface in two experiments performed as in Fig. 1 on curing epoxy.
- Fig. 4. Impedance ratios computed from the data of Fig. 3. See Table I for absolute values.
- Fig. 5. Block diagram of the instrumentation used for waves in wires. Specimens and thermocouples were dipped vertically into vials of epoxy.
- Fig. 6. Echoes (upper) and Selector Monitor pips (lower) photographed on the CRO, and corresponding specimen geometry, in one experiment performed with equipment in Fig. 5 with specimen immersed.
- Fig. 7. Data on a wire specimen in epoxy, during curing.
- Fig. 8. Amplitude of the meniscus echo from a lead-in wire (without specimen) held in epoxy during curing.
- Fig. 9. Test set to monitor polymerization automatically. The amplitude outputs A and B were from the weld (II) and the specimen end (III) respectively at first. When the meniscus echo (I) grew to a preset trigger level channel A began monitoring the meniscus (I) and channel B switched to the weld (II).
- Fig. 10. Data from the test set in Fig. 9. When the meniscus echo reached the trigger level, channels A and B switched from positions II and III to positions I and II of Fig. 9.

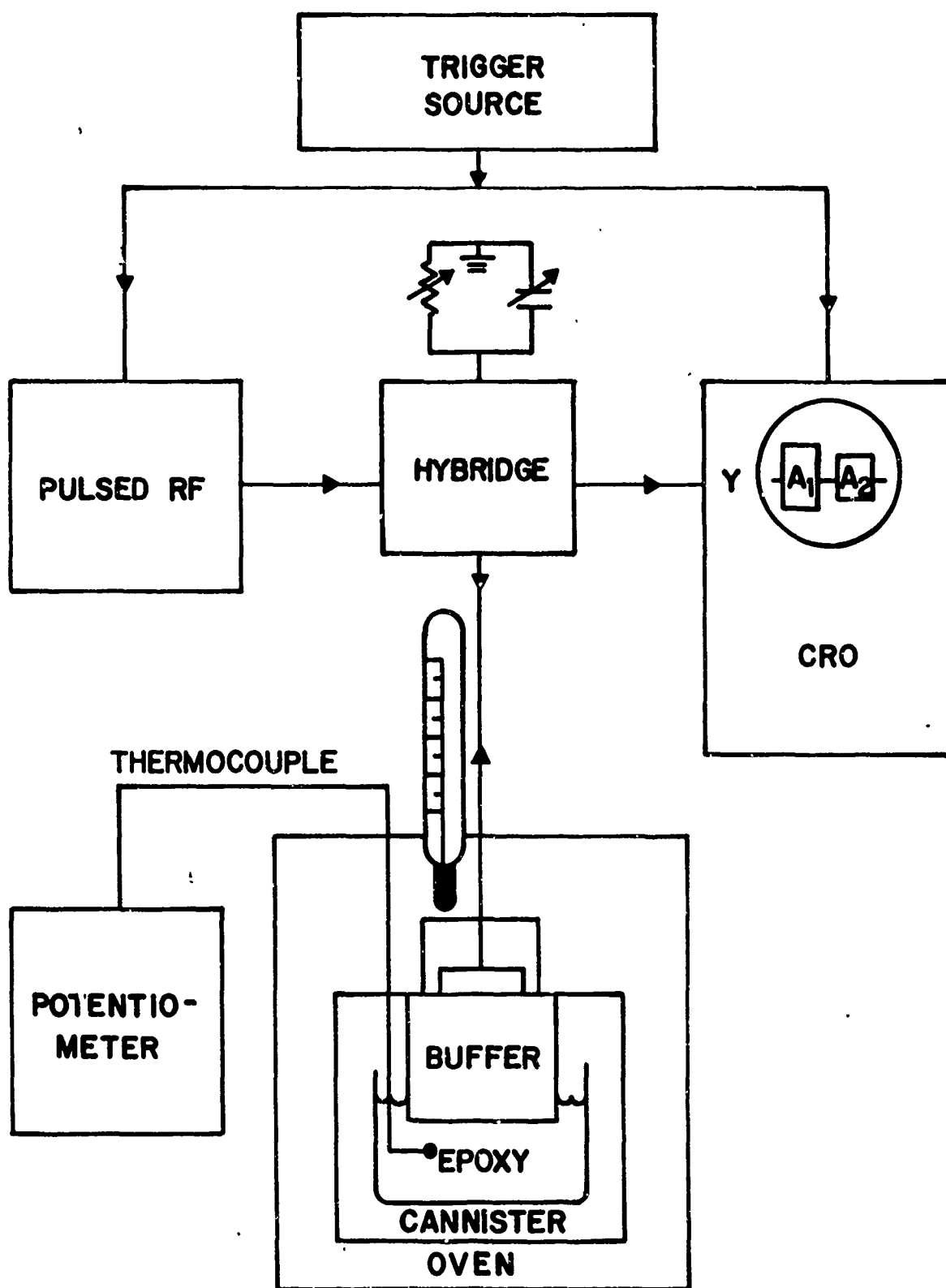


FIGURE 1

A11

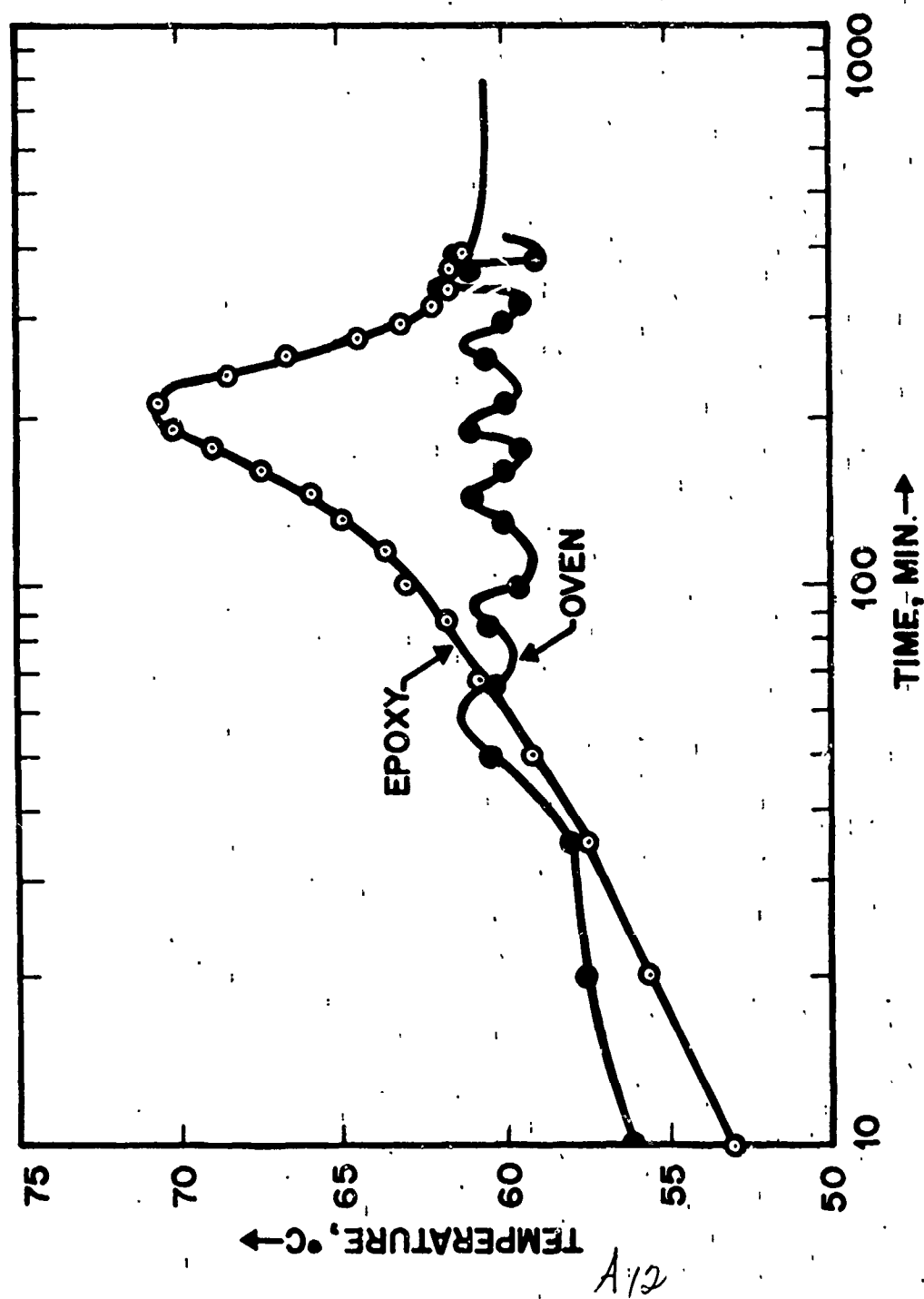
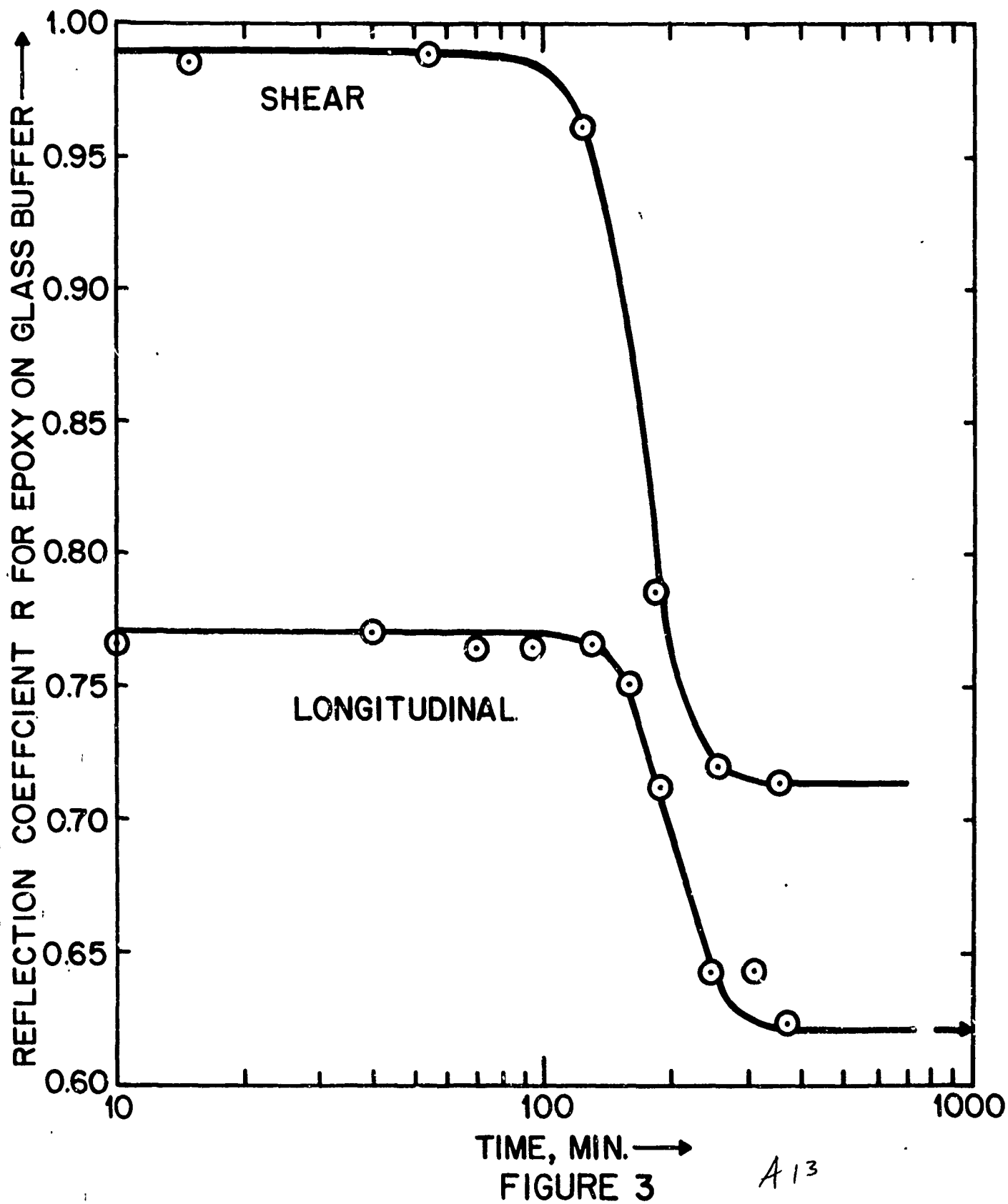


FIGURE 2

A12



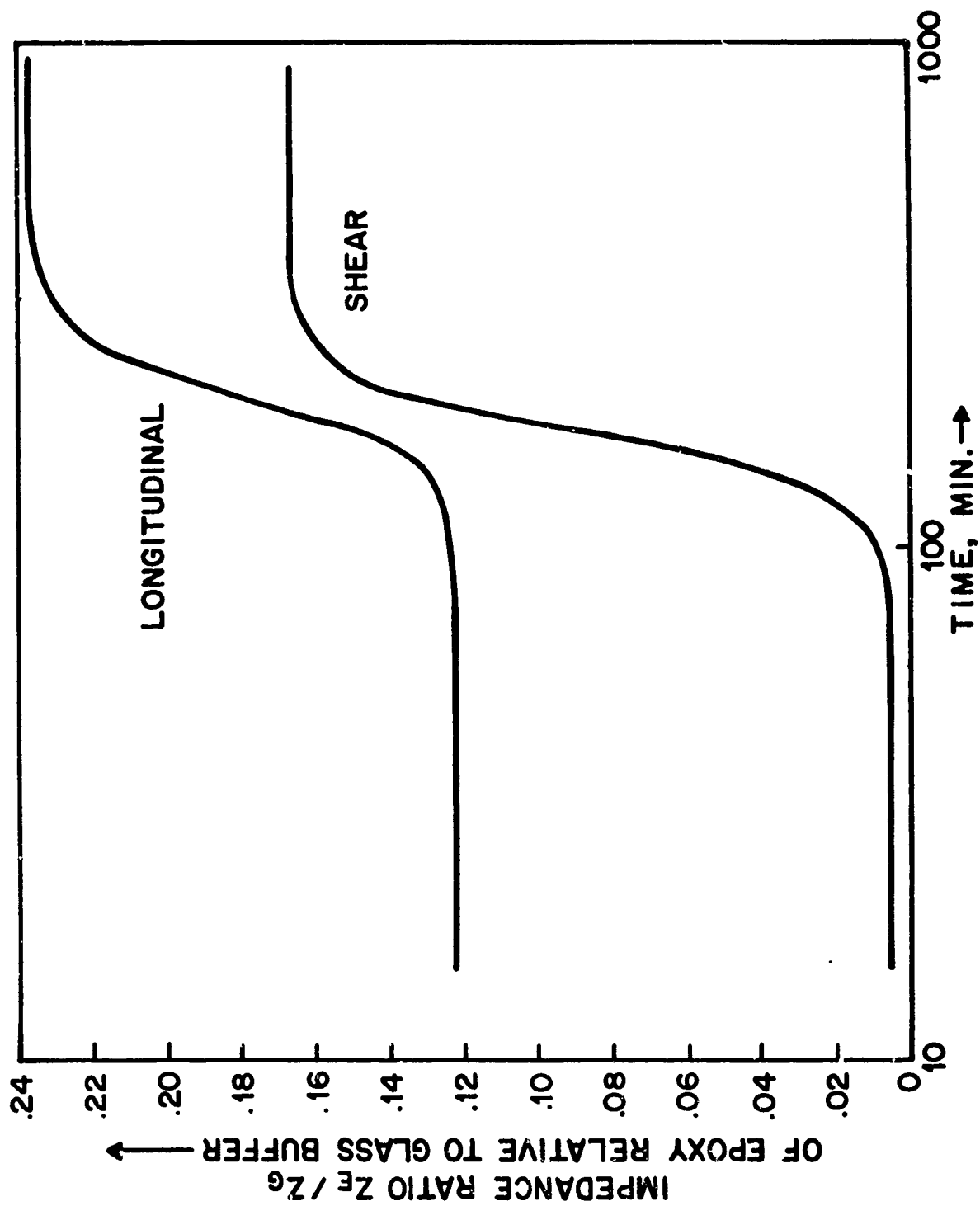


FIGURE 4

A14

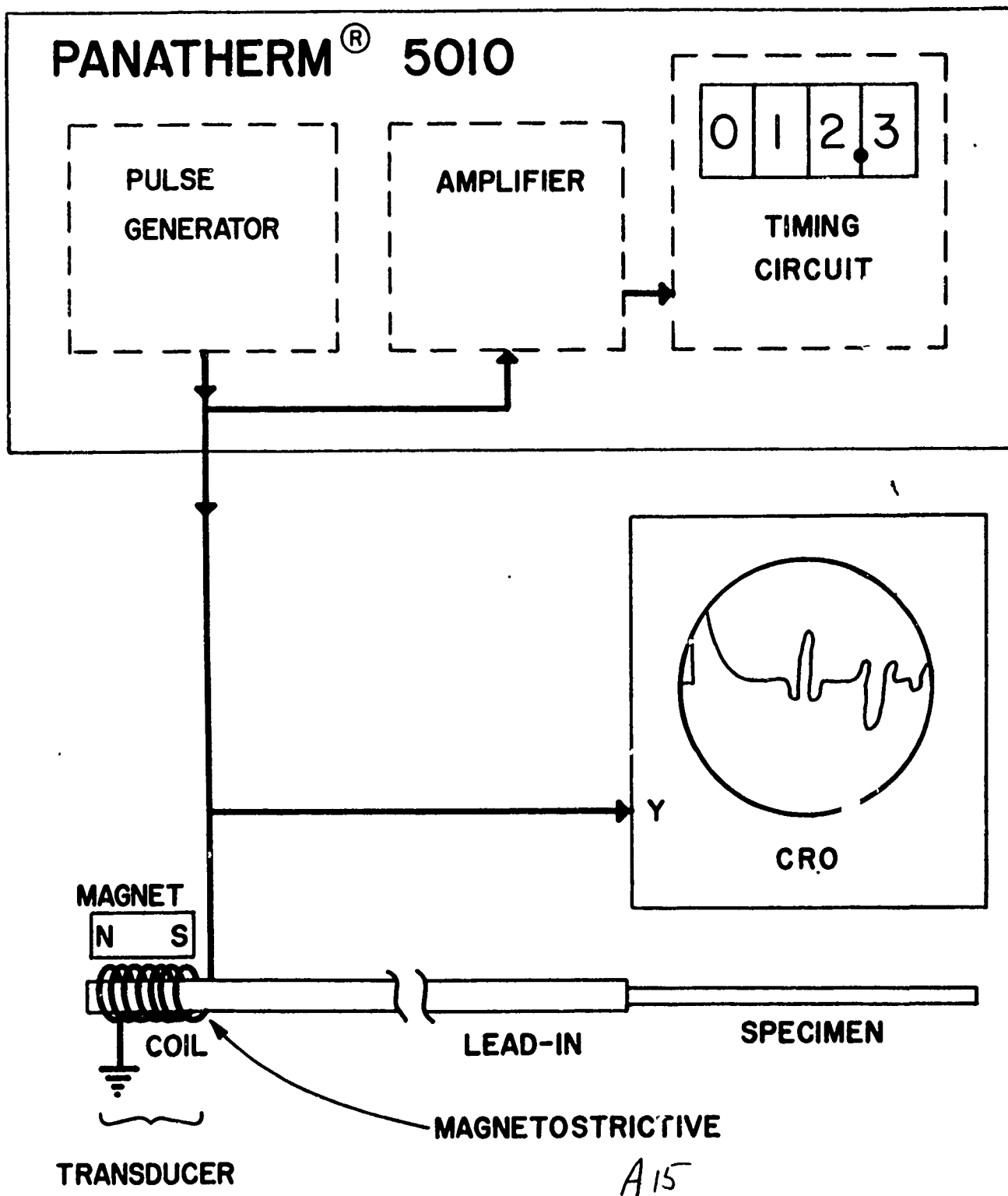
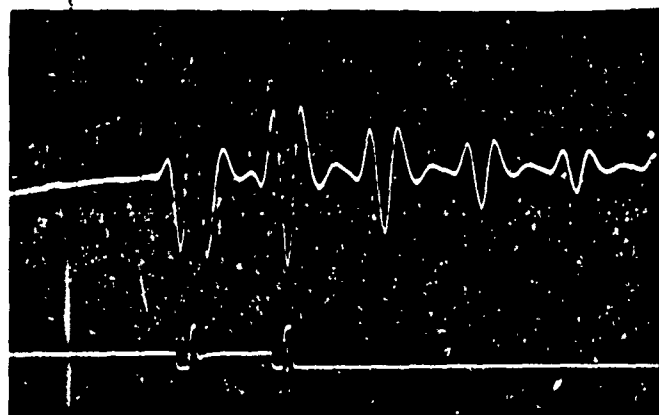
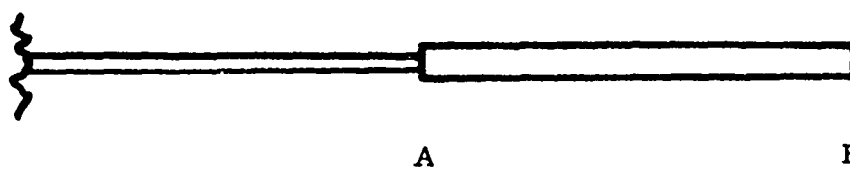


FIG. 5



PANATHERM® ECHOES SHOWING
SELECTOR MONITOR GATES
POSITIONED AT A AND B



A16

FIG. 6

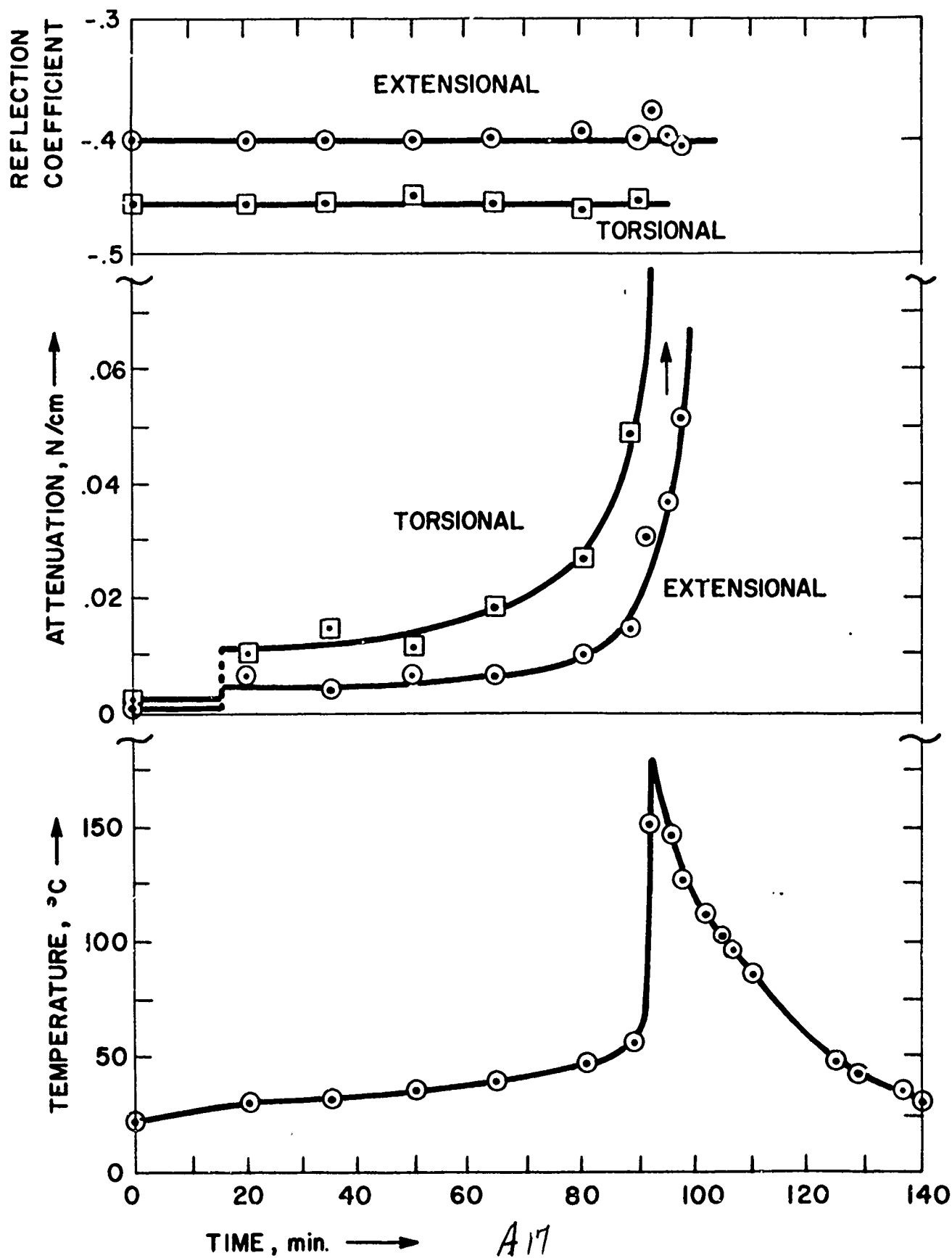


FIG. 7

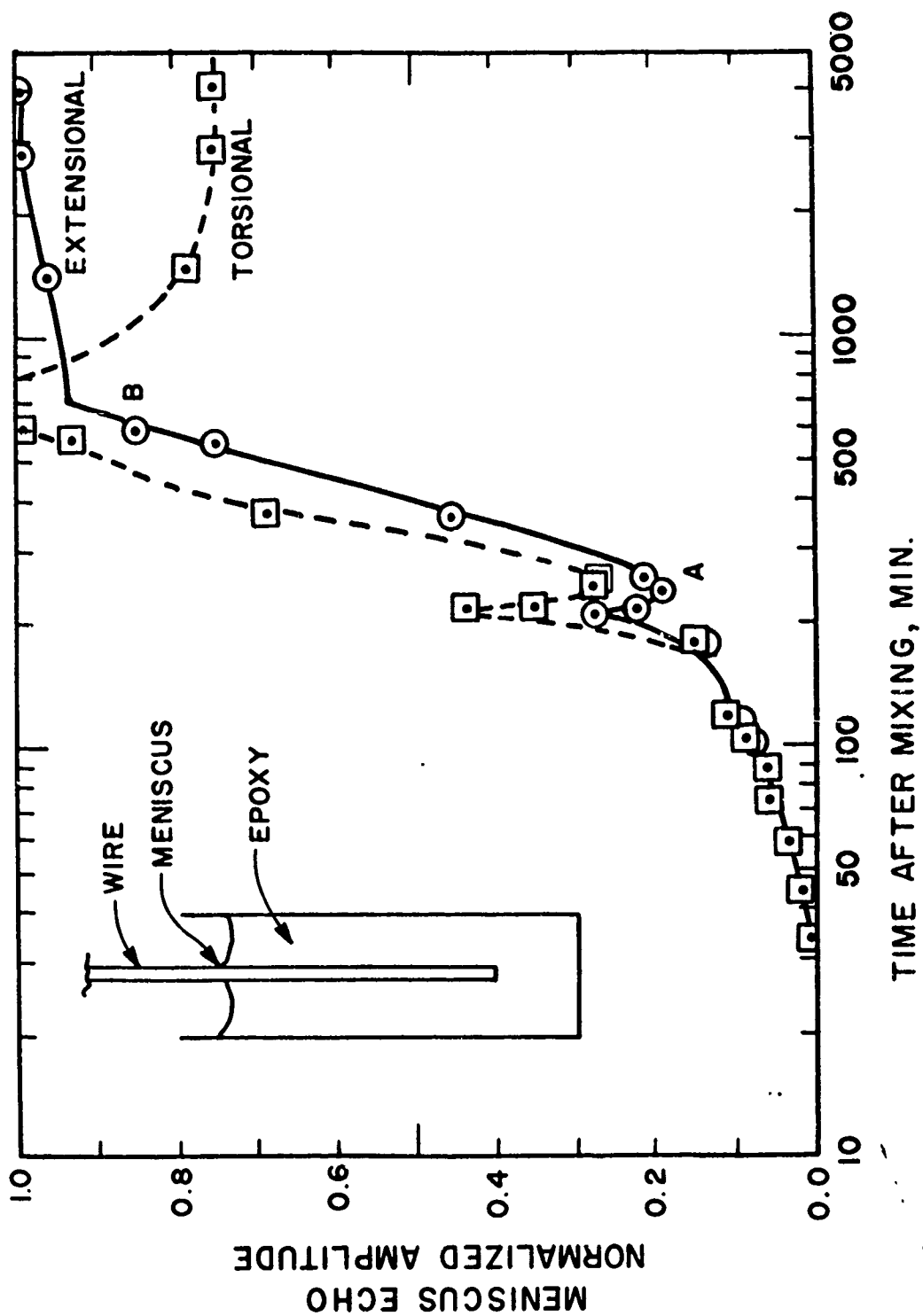
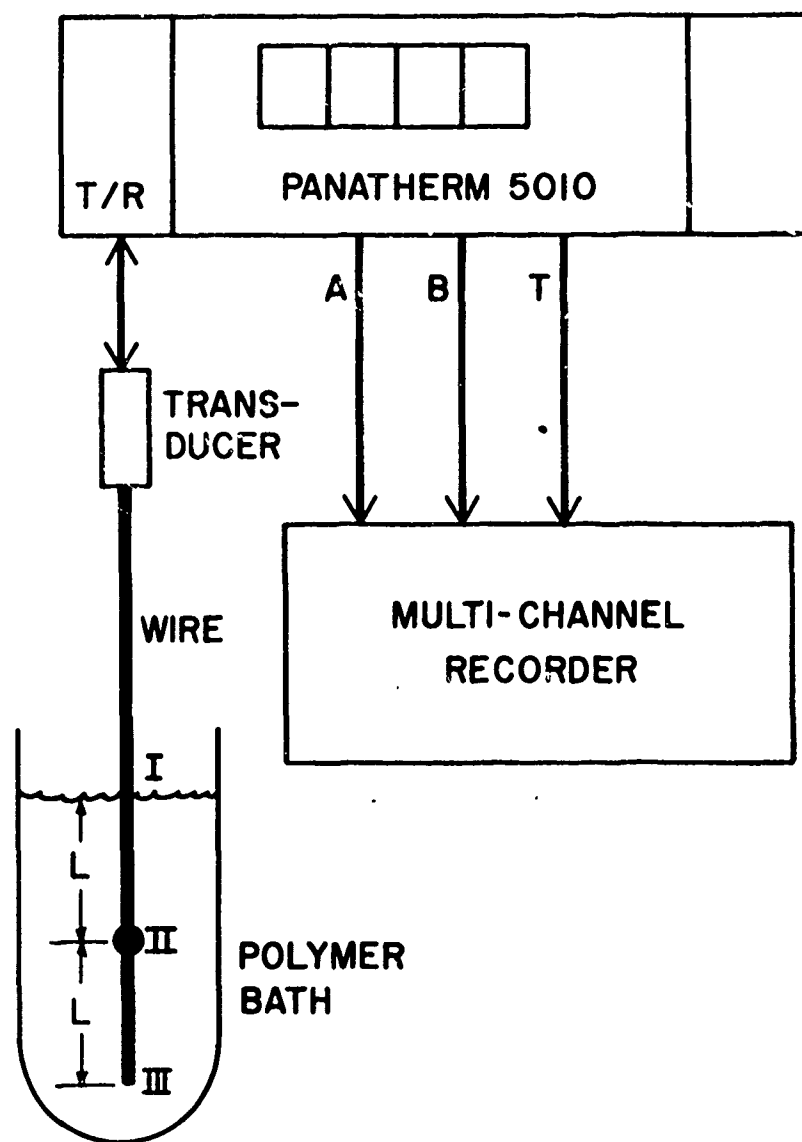


FIG. 8

A18



A19

FIG. 7

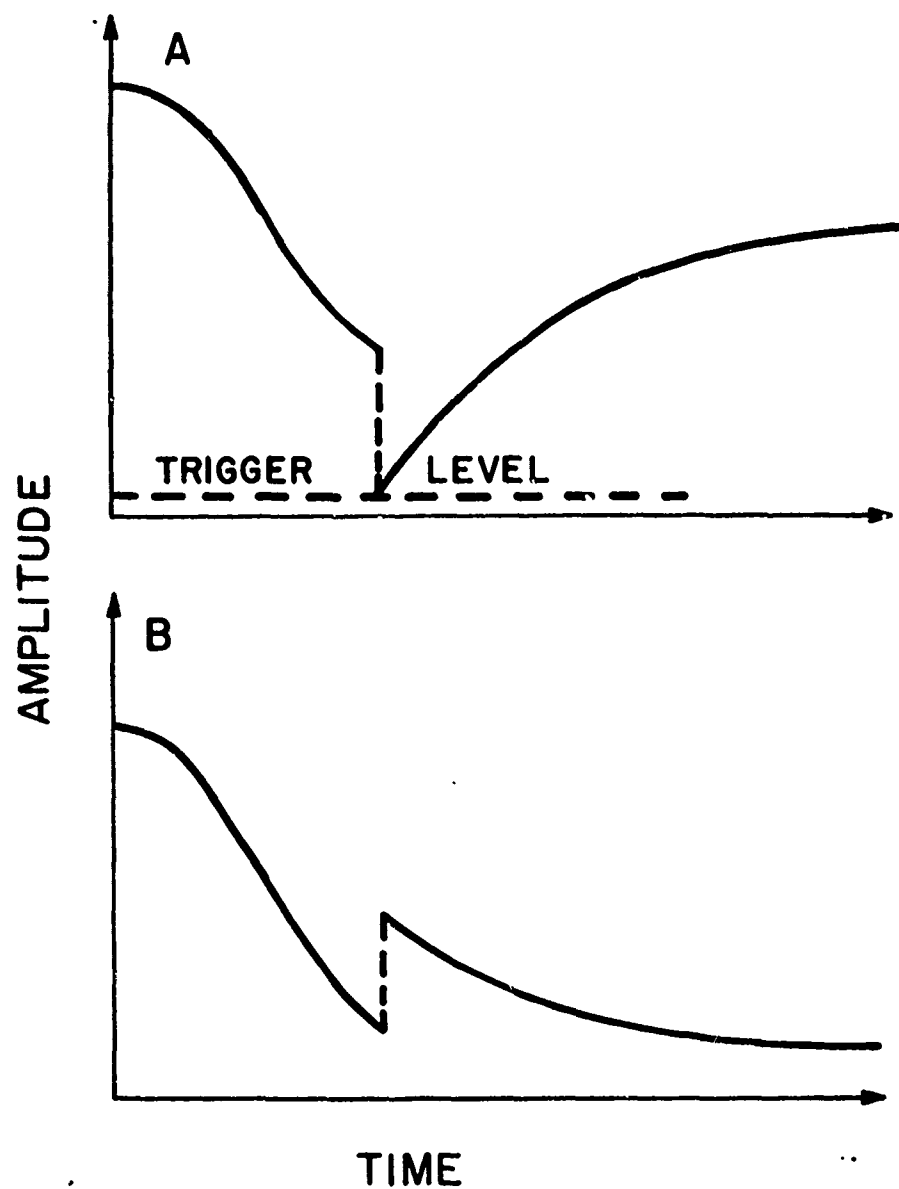


FIG. 10

A20

APPENDIX B

Attenuation and Reflection Coefficient Nomogram

by
Lawrence C. Lynnworth

In determining the attenuation coefficient α (Np/unit length) using the pulse-echo buffer rod technique, calculations usually involve three echoes, such as the interface echo A and the free back surface echoes B and C. Appropriate formulas have been derived by Papadakis,⁽¹⁾ taking into account the sound pressure reflection coefficient R at the buffer/specimen interface. These formulas usually are written in terms of normalized echo amplitude ratios such as $\bar{A} \equiv A/B$ and $\bar{C} \equiv C/B$ with signs preserved, and the specimen length L:

$$|R| = [\bar{A} \bar{C} / (\bar{A} \bar{C} - 1)]^{1/2} \quad (1)$$

and

$$\alpha = [\ln (R/\bar{C})] / 2L. \quad (2)$$

The sign of R is the same as that of \bar{C} , in the present notation. As a cross check, the sign of R can be found from the impedances Z_1 and Z_2 of the buffer and specimen as

$$R \text{ positive when } Z_2 > Z_1; \quad (3)$$

$$R \text{ negative when } Z_2 < Z_1.$$

For highest accuracy, A, B and C may be corrected for diffraction prior to evaluating α and R by these formulas.⁽²⁾ They should also be corrected for nonlinearities in the transducer and electronic amplifiers.

In some cases it is convenient, and sufficiently accurate, to determine $2\alpha L$ and R graphically from a log-log nomogram. One such nomogram is constructed by plotting iso- α curves and iso-R lines as functions of \bar{A} and \bar{C} . As a numerical example, if $\bar{A} = 10$ and $\bar{C} = -0.1$, we estimate $2\alpha L \approx 2$ Np and $|R| \approx 0.7$. (More exact values, computed using (1) and (2), are: $|R| = 0.7071$, $2\alpha L = 1.956$ Np ≈ 17 dB.)

References

1. E. P. Papadakis, Buffer-Rod System for Ultrasonic Attenuation Measurements, J. Acoust. Soc. Amer. 44 (5), 1437-1441 (Nov. 1968); E. P. Papadakis, Traveling Wave Reflection Methods for Measuring Ultrasonic Attenuation and Velocity in Thin Rods and Wires, J. Appl. Phys. 42 (7), 2990-2995 (June 1971). In special cases where R is known or measurable without recourse to C, simpler expressions may be derived for α . See, for example, L. C. Lynnworth, Attenuation Measurements Using the Pulse-Echo AB Method, Without Multiple Echo Reverberations in Specimen, Materials Evaluation 29 (2), 27A (Feb. 1971); *ibid*, 31 (1 or 2) (Jan. or Feb. 1973); E. P. Papadakis et al., Ultrasonic Attenuation and Velocity in Hot Specimens by the Momentary Contact Method with Pressure Coupling, and Some Results on Steel to 1200°C, J. Acoust. Soc. Amer. 52 (3) Pt. 2, 850-857 (Sept. 1972).
2. E. P. Papadakis, K. A. Fowler and L. C. Lynnworth, New Uses of Ultrasonic Spectrum Analysis, in: 1972 Ultrasonics Symp. Proc., IEEE Cat. #72 CHO 708-8SU, IEEE, New York, 1972, pp. 81-86. For an explicit treatment of the diffraction correction for bulk waves, see: E. P. Papadakis et al., Ultrasonic Attenuation by Spectrum Analysis of Pulses in Buffer Rods: Method and Diffraction Corrections, J. Acoust. Soc. Amer. (to be published).

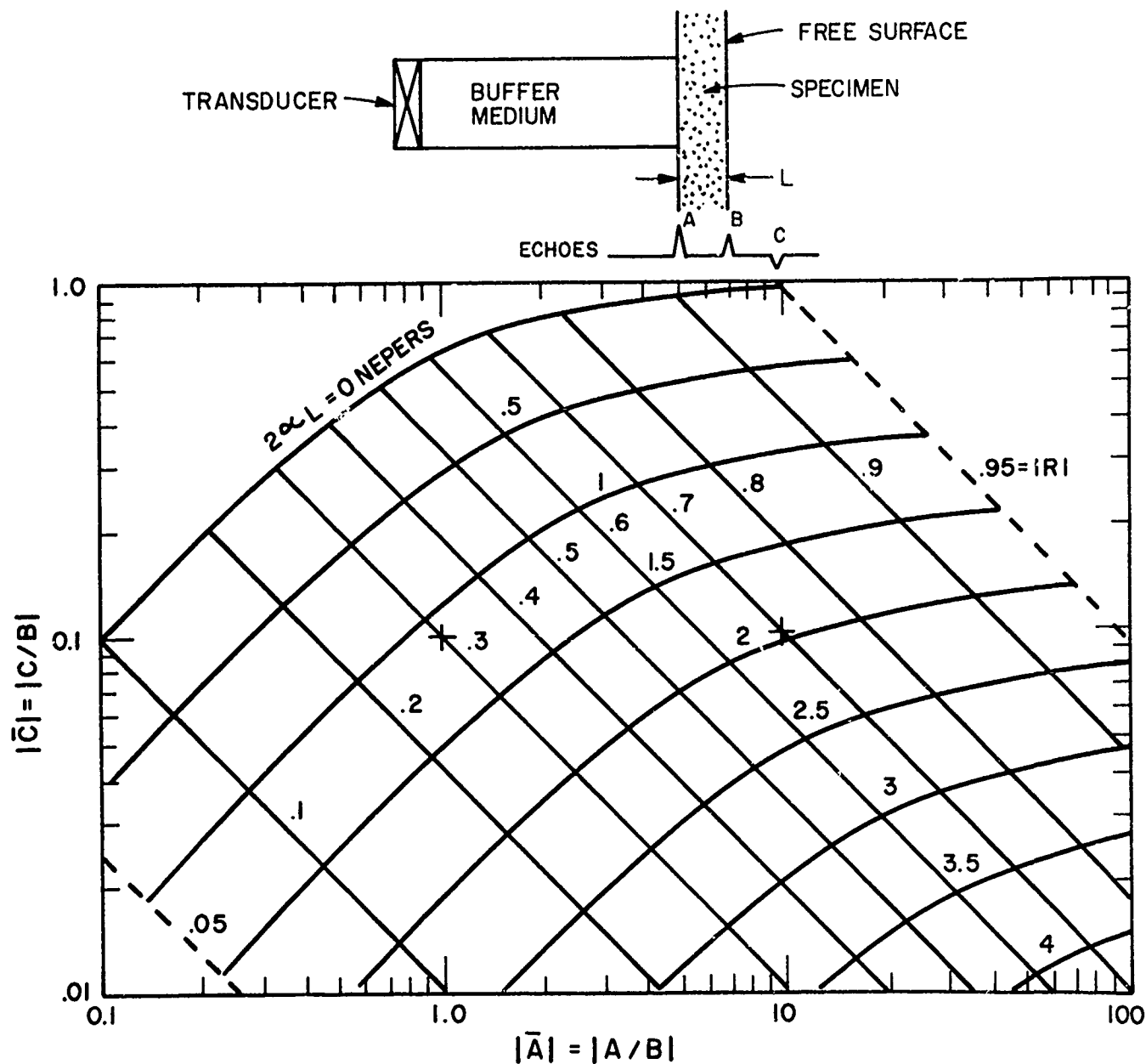


Fig. 1. Nomogram for finding specimen loss and reflection coefficient at the end of a buffer rod from the amplitudes of the first three echoes as corrected for beam spreading when present, and transducer and electronic nonlinearity when present.



PANAMETRICS

221 Crescent Street • Waltham, Massachusetts 02154 • (617) 899-2719

Ultrasonic Methods for Modulus Measurement
in Paper^{*}

Emmanuel P. Papadakis, Ph.D.

Presented at the 1972 Testing Conference of the Technical Association
of the Pulp and Paper Industry, Benjamin Franklin Hotel, Philadelphia,
Pennsylvania, September 26-29, 1972.

Technical Memorandum No. 8

C-1

^{*}This work was supported in part by the Office of Naval Research,
Acoustics Branch.

I INTRODUCTION

My subject today is the modulus of paper, and two ultrasonic methods to measure it on-line.

Modulus is related to strength and to bending stiffness. (M. Jackson and G. Gavelin, *Svensk Pappers Tidning* 70, 63 (1970).) The latter is proportional to Young's modulus, and the former can be correlated with it. It would be advantageous to be able to measure, on-line, a quantity which is a function of Young's modulus.

II. PLATE WAVE THEORY

One such quantity is the velocity V_p of the first longitudinal plate wave in the paper. This wave velocity occurs when the paper is much thinner than one ultrasonic wavelength.

The modes in plates are illustrated in Slide 1. (First slide, please.) The wave velocity is in the direction of the vector V , while the particle motion directions are shown by the short arrows. The first longitudinal mode, the first flexural mode, and the zeroth shear mode are shown.

The group delay (or travel time) of modes in plates are illustrated in Slide 2. (Next slide, please.) The group delay D of wave pulses is plotted against frequency f . Both quantities are normalized with respect to thickness and velocity to be dimensionless. The plate velocity V_p is indicated at the lower end of the first longitudinal mode curve. This is the fastest mode in the plate, showing the shortest delay D . The velocity is given by the equation

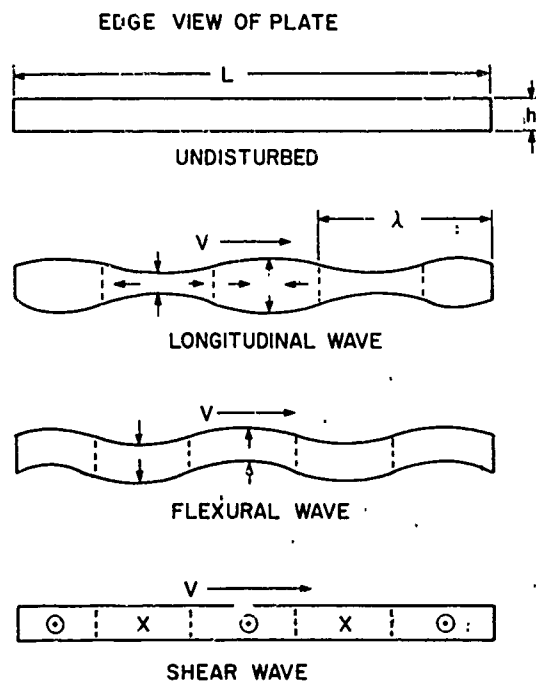
$$V_p = [Y/\rho (1 - \sigma^2)]^{1/2} \quad (1)$$

where ρ is density, σ is Poisson's ratio, and Y is Young's modulus. Other relevant equations are shown in Slide 3. (Next slide, please.)

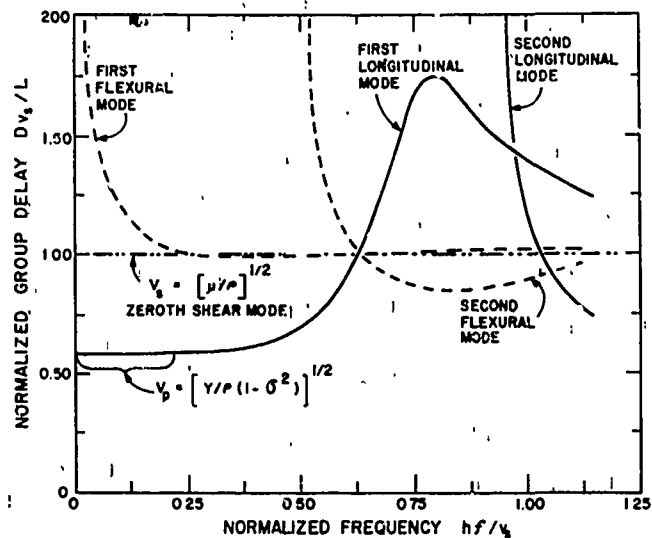
This formula for V_p is not ideal because it depends on Poisson's ratio as well as on Young's modulus. However, Poisson's ratio may be expressed as

$$\sigma = Y/2\mu - 1 \quad (2)$$

where μ is the modulus of rigidity. The rigidity modulus may be found by propagating a shear wave in the plate. The velocity V_s of the zeroth

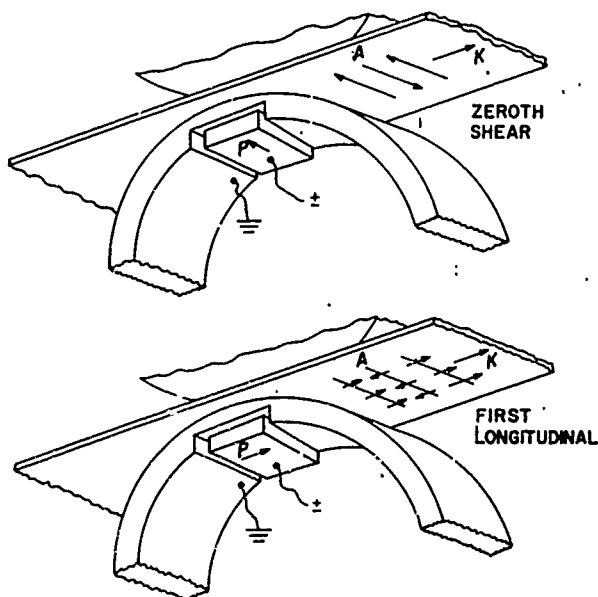


Slide 1. Illustration of motion of lowest modes in plates.

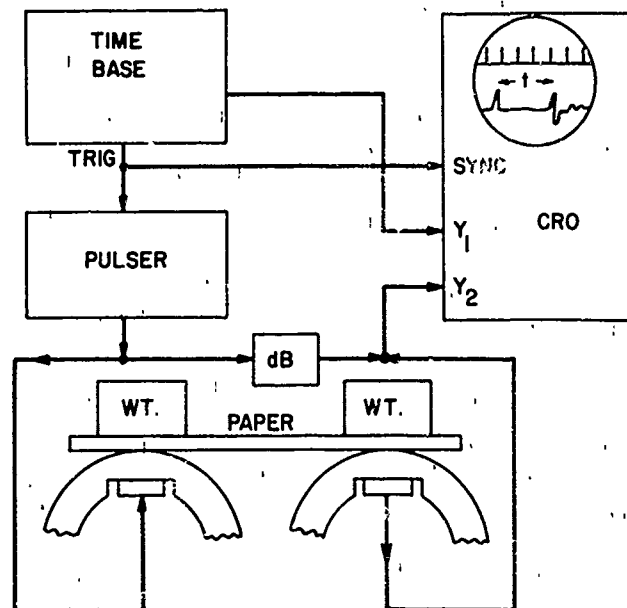


Slide 2. Group delay of some low modes in isotropic plates.

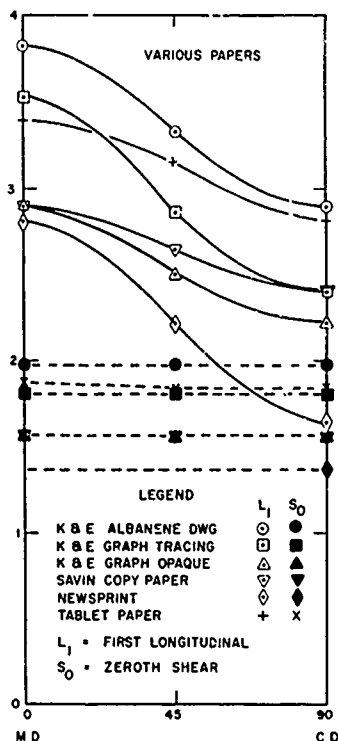
Slide 3. Slide 3 contained Equations (1) through (5) in the text.



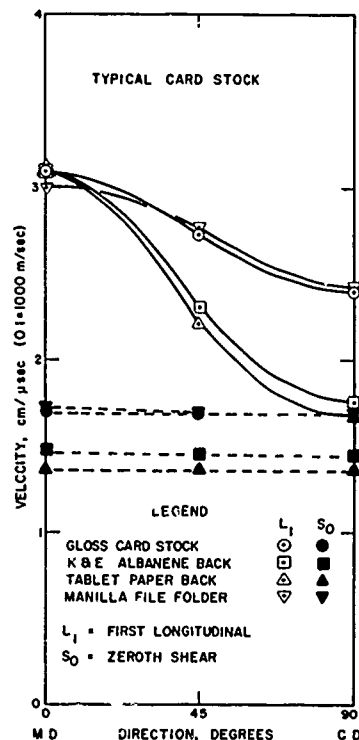
Slide 4. Wheel transducers with piezoelectric elements for generating longitudinal and shear wave beams in plates.



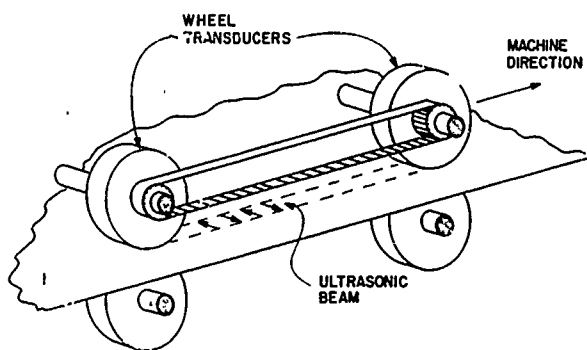
Slide 5. Instrumentation for velocity measurements in paper with wheel-type transducers.



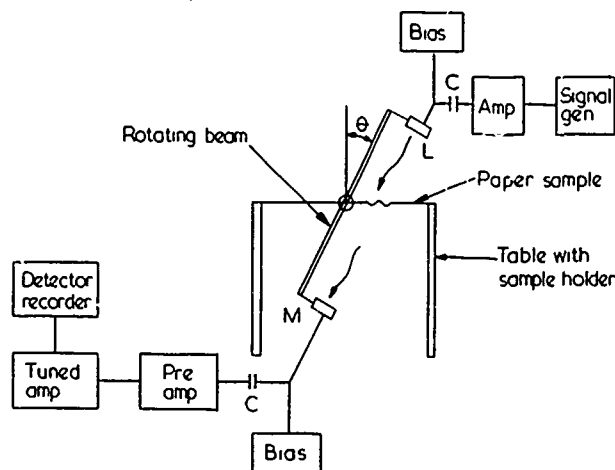
Slide 6. Velocity in paper for first longitudinal and zeroth shear modes by wheel method.



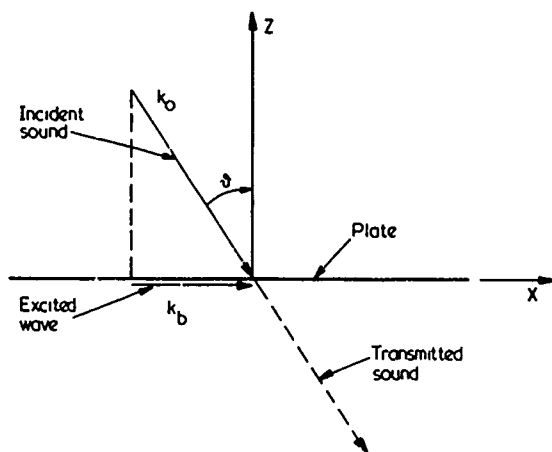
Slide 7. Velocity in card stock for first longitudinal and zeroth shear modes by wheel method.



Slide 8. Synchronous wheel transducer configuration for measuring velocity in sheet material on-line.

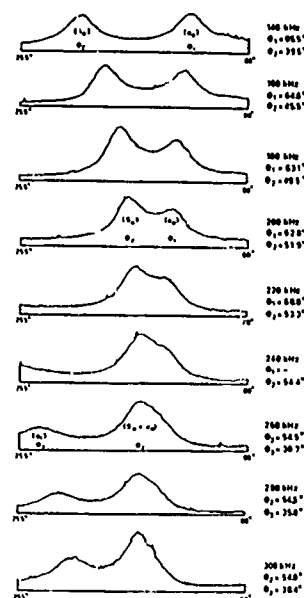


Slide 9. Noncontacting experiment on velocity in paper. Transmission through the paper occurs when plate waves are excited in it. (Luukkala et al., Ultrasonics 9, 201-208 (1971).)



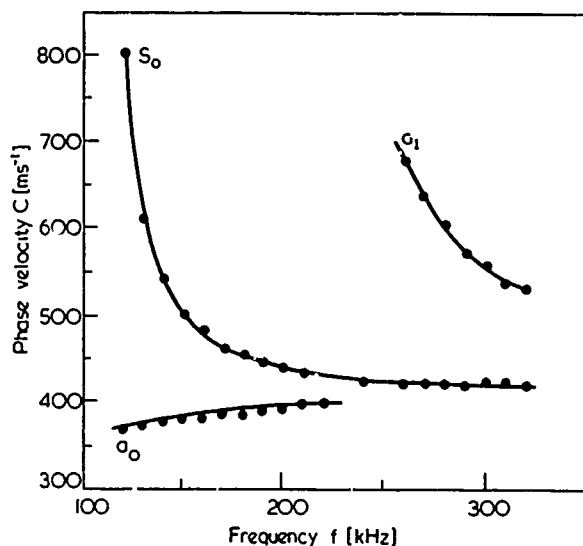
$$k_0 \sin \theta_k = k_b, \text{ or } C_0 = C_b \sin \theta_k$$

Slide 10. Wavelength matching condition for transmission through the paper. (Luukkala et al., op. cit.)

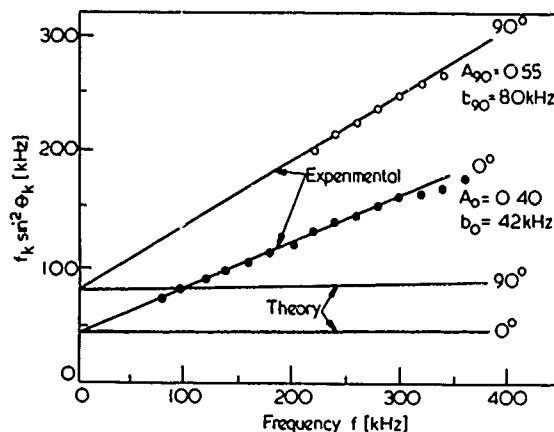


Slide 12. Amplitude versus angle for several frequencies by the non-contacting method in card 0.85 mm thick. Maximum signal occurs at the wavelength matching condition which excites a plate wave. (Luukkala et al., op. cit.)

Slide 11. Slide 11 contained Equation (8) in the text.



Slide 13. Mode curves of phase velocity versus frequency computed by Equation (6) from the data of Slide 12. (Luukkala et al., op. cit.)



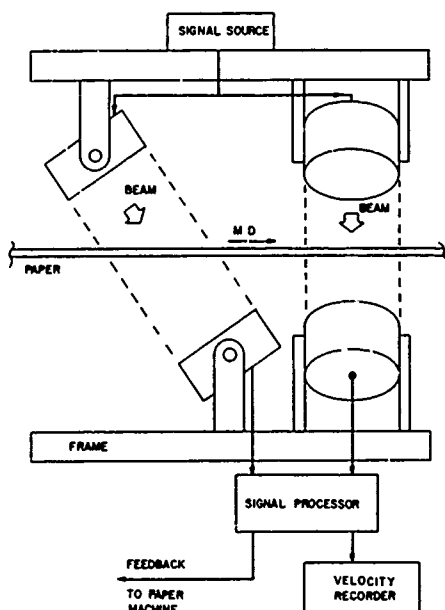
$$f_k \sin^2 \theta_k = \frac{C_0^2(1+\nu)}{C_L^2(2(1-\nu))} \cdot f_k + \frac{C_0^2\sqrt{3}}{\pi d C_L}$$

Slide 14. Extrapolation of data to low-frequency limit to get plate velocity V_p of Equation (1). (Luukkala et al., op. cit.)

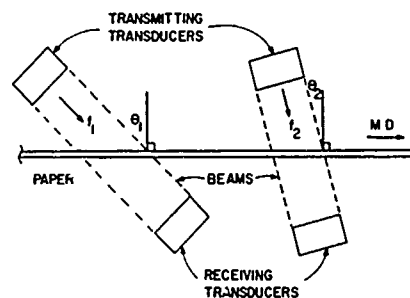
Table 1 Comparison between the two methods (0 = machine direction, 90 = transverse direction, x = measurement could not be carried out)

Sample code	Plate wave resonance			Dynamic modulus tester		
	C_{L0} [ms ⁻¹]	C_{L90} [ms ⁻¹]	AI	C_{L0} [ms ⁻¹]	C_{L90} [ms ⁻¹]	AI
S1-1	1890	1530	1,23	1980	1570	1,26
S1-2	1930	1850	1,06	2070	1720	1,22
S1-3	1930	1550	1,26	2000	1830	1,06
S2-1	2200	1490	1,48	3050	2300	1,33
S5-1	4800	x	x	3530	2020	1,75
S5-2	3320	x	x	3900	2000	1,95
S5-3	2790	x	x	3530	1950	1,81
S6-1	1710	1380	1,24	2120	1580	1,34
S6-2	1960	1280	1,53	2660	1650	1,61
S6-3	1720	1460	1,15	1610	1540	1,05
C185	2760	1870	1,48	3260	2220	1,47
C74	3020	2000	1,5	3140	2600	1,21
C427	2670	x	x	2980	2490	1,20
B638	2780	2410	1,15	3290	2840	1,16
B1572	3940	2600	1,51	x	x	x
K	4000	2790	1,44	4450	2440	1,82
B1	3100	x	x	3100	1380	2,35
B2	4100	2410	1,70	4200	1820	2,31
B3	3830	2020	1,91	3770	1940	1,94

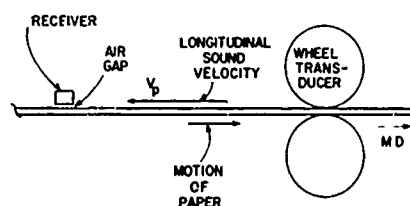
Slide 15. Extrapolated results compared with data from dynamic modulus tester. (Luukkala et al., op. cit.)



Slide 16. Conceptual sketch of on-line modulus tester for sheet material employing noncontacting method.



Slide 17. Noncontacting test set-up with two pairs of transducers at two angles and radiating at two frequencies for a dispersive wave mode.



Slide 18. Contact wheel transducer radiating in untouched paper to a noncontacting receiver.

be done directly by rotating the transducers, or it could be done indirectly by varying the frequency fed to a phased array transducer. Physical angle or frequency would have to be varied with a feedback mechanism to hunt for maximum transmission. The hunt for maximum transmission could be complicated by various ambient factors such as turbulent air or absorption in the paper.

Ordinary plane transducers could be used in the noncontacting case if one chose to operate in a dispersive region of the longitudinal mode. For each direction of interest, e. g. , the machine direction, two pairs of transducers would be needed. See Slide 17. (Next slide, please.) The two pairs would be set at different angles of incidence, and the input frequency to each pair would be different and would be swept independently to find maximum transmission for each pair. The resultant velocity of plate waves would be found by extrapolating a plot of $f \sin^2 \theta$ versus f to zero frequency as shown earlier in Slide 14. A single system to monitor frequency at a single angle might be adequate for practical purposes.

The contact method seems attractive at first glance if contact were permissible. Turbulent air problems are absent, and absorption in the paper would not be a problem as long as signal strength did not fall below a threshold. However, the rolling action under pressure might modify the paper being measured. This problem might be overcome with an air-coupled transducer as receiver "upstream" from the wheel transmitter. See Slide 18. (Next slide, please.) The virtue of this configuration would be that paper untouched by the wheel roller would be interrogated.

In summary, on-line modulus monitoring of paper is now within the realm of possibility. Work is still necessary to define the best method to use, and the best configuration to exploit the method. A close interaction between producers and experimenters will be necessary to create a viable system.